Relocation of rDNA repeats for repair is dependent on SUMO-mediated nucleolar release by the Cdc48/p97 segregase

Matías Capella[1,2], Imke K. Mandemaker[1], Lucía Martín Caballero[1,3], Boris Pfander[3,4], Andreas G. Ladurner[1,3], Stefan Jentsch[2,†], and Sigurd Braun[1,3,*]

[1]Department of Physiological Chemistry, Biomedical Center (BMC), Ludwig Maximilians University of Munich, Martinsried, Germany
[2]Max Planck Institute of Biochemistry, Molecular Cell Biology, Martinsried, Germany
[3]International Max Planck Research School for Molecular and Cellular Life Sciences, Martinsried, Germany
[4]Max Planck Institute of Biochemistry, DNA Replication and Genome Integrity, Martinsried, Germany
[†]Deceased during the course of this study

[*]Correspondence:
sigurd.braun@bmc.med.lmu.de
Tel: +49 (89) 2180 77128

Keywords
Ribosomal DNA, genome stability, chromosome dynamics, SUMOylation, phosphorylation.

Abstract

Ribosomal RNA genes (rDNA) are highly unstable and susceptible to rearrangement due to active transcription and their repetitive nature. Compartmentalization of rDNA in the nucleolus suppresses uncontrolled recombination. However, broken repeats must be released to the nucleoplasm to allow repair by homologous recombination. The process of rDNA relocation is conserved from yeast to humans, but the underlying molecular mechanisms are currently unknown. Here we show that DNA damage induces phosphorylation of the CLIP component Nur1, releasing nuclear membrane-tethered rDNA repeats from the nucleolus in *Saccharomyces cerevisiae*. Cooperating with Nur1 phosphorylation, SUMOylation targets the rDNA tethering complex for disassembly mediated by the segregase Cdc48/p97, which recognizes SUMOylated CLIP-cohibin through its cofactor, Ufd1. Consistent with the conservation of this mechanism, UFD1L depletion impairs rDNA release in human cells. The dynamic and regulated assembly and disassembly of the CLIP-cohibin complex is therefore a key, conserved determinant of nucleolar rDNA release and genome integrity.

Introduction

Eukaryotic genomes contain large amounts of repetitive sequences at centromeres, telomeres, and ribosomal RNA genes (rDNA). In *Saccharomyces cerevisiae*, the rDNA locus consists of approximately 150 copies, organized in 9.1 kb tandem repeats on chromosome XII. Humans have hundreds of 43 kb rDNA units located on different chromosomes. This large availability of donor sequences means that rDNA repeats often undergo homologous recombination (HR), making them a major source of genome instability (Kobayashi, 2011). As an example, DNA double-strand break (DSB) repair within a repetitive array can cause repeat insertions or deletions through HR with a neighboring unit (Jaco et al., 2008; Kobayashi, 2011; Kobayashi et al., 2004). Such rearrangements can have severe consequences. Indeed, rDNA repeat translocations are associated with cellular senescence, neurodegenerative diseases, and are amongst the most common events observed in cancer cells (Hallgren et al., 2014; Lindström et al., 2018; Sinclair and Guarente, 1997; Stults et al., 2009; Udugama et al., 2018).

The rDNA repeats are spatially segregated into the nucleolus, a membrane-less subnuclear organelle. In *S. cerevisiae*, rDNA is tethered to the nuclear envelope by the CLIP (chromatin linkage of inner nuclear membrane proteins) and the cohibin complexes (Mekhail et al., 2008). Cohibin is a “V”-shaped complex composed of one Lrs4 homodimer and two Csm1 homodimers. It associates with rDNA through its interaction with the RENT complex (regulator of nucleolar silencing and telophase exit) and Tof2 (Corbett et al., 2010; Huang et al., 2006; Mekhail et al., 2008). Cohibin tethers rDNA to the nuclear periphery by binding the CLIP complex. CLIP comprises two integral inner nuclear membrane proteins, the LEM domain protein Heh1 (also known as Src1) and Nur1 (Figure S1A) (Mekhail et al., 2008).

SUMOylation plays multiple roles in DNA damage repair. Akin to ubiquitylation, an enzymatic cascade covalently attaches the small ubiquitin-like modifier SUMO to specific lysine residues on target proteins. SUMO and its conjugates are recognized by proteins containing SIMs (SUMO interacting motifs) (Geiss-Friedlander and Melchior, 2007). Furthermore, several SUMO moieties can be conjugated to form a chain, which triggers protein degradation through the recruitment of SUMO-targeted ubiquitin ligases (STUbLs) (Prudden et al., 2007). Conversely, SUMO moieties can be removed by the SUMO-specific proteases Ulp1 and Ulp2, which also mediate

SUMO maturation by exposing the C-terminal Gly-Gly motif (Geiss-Friedlander and Melchior, 2007).

SUMOylation of Rad52, a key player in DSB repair, is one of an array of mechanisms that suppresses aberrant rDNA repeat recombination (Mekhail et al., 2008; Torres-Rosell et al., 2007). Together with the Smc5/6 (structural maintenance of chromosomes) and MRX (Mre11-Rad50-Xrx2) complexes, SUMOylation prevents Rad52 from forming nucleolar foci (Torres-Rosell et al., 2007). Nucleolar Rad52 localization is further prevented by condensin-mediated rDNA condensation and RNA polymerase I transcription (Tsang and Zheng, 2009). Conversely, CLIP or cohibin disruption promotes rDNA release and aberrant recombination (Mekhail et al., 2008).

Keeping rDNA repeats within the nucleolus prevents aberrant recombination between different units; however, this spatial confinement presents a threat when cells encounter DNA damage. Damaged rDNA repeats need to be released from the nucleolus for repair by the HR machinery, and re-enter once fixed (Harding et al., 2015; van Sluis and McStay, 2015; Torres-Rosell et al., 2007). Similarly, repair of centromeric heterochromatin is blocked by Smc5/6-dependent exclusion of Rad51 in *Drosophila* and mouse cells, and its recovery involves the relocation of the damaged locus outside the heterochromatin domain (Chiolo et al., 2011; Tsouroula et al., 2016).

In addition to excluding Rad52 from the nucleolus, SUMO also mediates relocation of unresolved DSBs and damaged heterochromatin to the nuclear periphery for DNA repair (Horigome and Gasser, 2016). However, while the molecular events in the relocation of centromeric heterochromatin and other damaged sites have been intensely studied (Churikov et al., 2016; Horigome et al., 2016; Kalocsay et al., 2009; Ryu et al., 2015), the mechanisms controlling the relocation of broken rDNA repeats have remained mostly elusive.

Here, we report the molecular events that regulate nucleolar rDNA release in *S. cerevisiae*. We find that a series of posttranslational modifications control association of key molecular players at the nuclear periphery. We show that blocking rDNA relocation using a constitutively bound CLIP-cohibin complex is detrimental for cell survival, even in the absence of external DNA damage. This result implies that CLIP-cohibin dissociation is dynamic. We find that Nur1 phosphorylation is a critical trigger for disruption of the CLIP-cohibin complex (hereafter referred to as rDNA tethering

complex). In addition, our data reveal that SUMOylation of CLIP-cohibin mediates movement of individual rDNA repeats out of the nucleolus. SUMOylated CLIP-cohibin recruits the Cdc48/p97 segregase to assist in the disassembly of the rDNA tethering complex, a mechanism conserved in human cells. We propose that phosphorylation and SUMOylation of the CLIP-cohibin complex facilitate the transient release of damaged rDNA repeats from the nucleolus to the nucleoplasm to allow DNA repair.

Results

Permanent rDNA tethering is detrimental for cell survival

Deletion of CLIP or cohibin causes rDNA release from the nucleolus, which is reminiscent of rDNA relocation observed during DNA damage repair (Mekhail et al., 2008; Torres-Rosell et al., 2007). We thus postulated that rDNA release requires dynamic dissociation of CLIP and cohibin. To test this hypothesis, we generated an inducible artificial tethering system by fusing Heh1 (CLIP) to GFP-binding protein (GBP) under the control of the *GAL1* promoter and expressing it with ^{GFP}Lrs4 (cohibin) (Figure 1A). Intriguingly, when induced by galactose, these fusion proteins caused a severe growth phenotype, implying that failure to dissociate the CLIP-cohibin complex is toxic for cells (Figure 1B, lane 4). A similar phenotype was observed when co-expressing GFP-fusions of the rDNA-bound proteins Net1 and Tof2 with Heh1-GBP (Figures 1A and 1B, lanes 6 and 8) (Huang et al., 2006). Expressing Heh1 directly fused to either Lrs4 or Tof2 also produced severe growth defects (Figure 1C, lanes 4 and 7). In contrast, perinuclear tethering of the unrelated genomic Gal4-DNA-binding domain did not affect growth (Figure 1C, lane 8). Notably, growth was fully restored by expression of linear Heh1-Lrs4 fusions with mutations preventing cohibin assembly (*lrs4 Δ1-35*) (Corbett et al., 2010) or impairing its interaction with downstream factors (*lrs4 Q325Stop*) (Johzuka and Horiuchi, 2009) (Figure 1C, lanes 5 and 6, respectively). We verified that all fusion variants displayed similar expression levels, excluding any lack of growth defect due to altered protein levels. The only exception was the expression of Heh1-Tof2, which was undetectable despite the substantial phenotype caused by its expression (Figure S1B). Moreover, the observed phenotypes correlated with the expression levels, as driving Heh1-Lrs4 expression with the weaker *GALS* promoter resulted in less pronounce growth defects (Figures S1C and S1D). Based on these observations, we conclude that cell viability critically depends on the dissociation of ribosomal repeats from the nuclear periphery and nucleolus, and dynamic CLIP-cohibin disassembly.

The Nur1 C-terminal domain mediates rDNA tethering complex association

To unveil the molecular mechanism that controls CLIP-cohibin disassembly, we dissected interactions within the rDNA tethering complex. Using co-

immunoprecipitation (coIP) assays, we found that deleting individual CLIP or cohibin components affects the binding of the two complexes. Specifically, Heh1 (CLIP) failed to interact with Csm1 (cohibin) in *lrs4*Δ or *nur1*Δ cells (Figures 2A and 2B). Moreover, Lrs4 (cohibin) interaction with Nur1 (CLIP) was abolished in cells lacking Csm1 (Figure S2A). These results indicate that the integrity of both complexes is required for CLIP-cohibin association. In contrast, Heh1 interaction with Nur1 was largely unaffected in the absence of Lrs4 (Figure S2B), revealing that CLIP formation is independent of cohibin integrity. In *S. cerevisiae*, *HEH1* is a rare example of alternative splicing, which generates a shorter version known as Heh1-S that does not bind Nur1 (Capella et al., 2020; Grund et al., 2008). We consistently detected Lrs4 binding to Heh1, but not Heh1-S, upon expression of an N-terminal GFP-Heh1 fusion that allows detection of both splice variants (Figure S2C).

Using yeast two-hybrid assays (Y2H), we mapped interactions between individual domains. We found that the N-terminal Heh1 domain is critical for Csm1 association, and the C-terminal Nur1 region interacts with both cohibin members (Figure 2C). Further analysis narrowed the Nur1 interaction interface with Csm1 down to the last 54 residues of the C-terminus (Figures 2D and S2D). Using coIP experiments, we confirmed the critical role of these residues for Nur1 association with Lrs4 *in vivo* (Figures 2E). Consistent with this, removal of the last residues also abolished Nur1 binding to Sir2 (Figures S2E), which associates with Nur1 through cohibin (Huang et al., 2006). In contrast, deletion of these C-terminal Nur1 residues does not impact CLIP complex formation (Figure S2E).

To monitor changes in the location of individual rDNA repeats, we used a yeast strain that harbors a tandem array of Tet-repressor-binding sites (224x*tetO*) inserted in the rDNA locus (Torres-Rosell et al., 2007). This strain also expresses TetI^{mRFP} to localize the modified rDNA unit as well as Rad52^{YFP} and Nop1^{CFP} to visualize Rad52 foci and the nucleolus, respectively (Figure 2F). Compared to WT cells, mutants lacking the Nur1 C-terminal domain or its last 54 residues displayed a marked increased in the number of cells with TetI^{mRFP} foci outside the nucleolus, reaching levels similar to *nur1*Δ cells (Figure 2G). From these data, we conclude that the most C-terminal region of Nur1 is required for CLIP-cohibin association.

Phosphorylation of the CLIP complex disrupts rDNA tethering

Nur1 was shown to be phosphorylated, and this modification is removed by the nucleolar phosphatase Cdc14 recognizing the C-terminal domain (Figure 2D) (Godfrey et al., 2015). As the C-terminal domain is also required for cohibin interaction, we tested whether phosphorylation triggers the disassembly of the rDNA tethering complex. Indeed, under conditions that favor the accumulation of phosphorylated Nur1, using either a thermosensitive mutant of Cdc14 (*cdc14-3*) or blocking globally dephosphorylation, we found, using coIP, that interaction of Nur1 with Lrs4 was reduced (Figures 3A and S3A). Conversely, depleting Net1, which inhibits Cdc14 phosphatase activity (Shou et al., 1999; Visintin et al., 1999), increased Nur1 interaction with Lrs4 (Figure S3B). To determine target sites in Nur1, we mutated several residues known to be phosphorylated to aspartic acid (D) (Holt et al., 2009) mimicking the modified state (Figure S3C). Notably, using Y2H assays, we found that the Nur1 interaction with Csm1 was abolished when residues S441, T446 and S449 were mutated to D, but unaffected when replaced by alanine (Figure S3D). We confirmed the critical role of these residues for the CLIP-cohibin interaction *in vivo* using coIP (Figure 3B).

Loss of perinuclear tethering causes destabilization of rDNA repeats, which can be quantitated by unequal sister-chromatid exchange (USCE) using the *ADE2* reporter gene inserted into the rDNA locus. When assessing the rate of *ADE2* gene loss in the *nur1* phosphomimic mutant, we found increased USCE similar to the *nur1*Δ mutant (Mekhail et al., 2008). This indicates that Nur1 phosphorylation decreases rDNA stability (Figure 3C). These results imply that the CLIP-cohibin association is dynamically controlled by Nur1 phosphorylation and counterbalanced by the phosphatase Cdc14.

CLIP-cohibin dissociation depends on SUMOylation

SUMOylation plays a prominent role in the DNA damage response and rDNA stability (Jalal et al., 2017). As the relocation of other genomic regions after damage requires SUMO (Horigome and Gasser, 2016), we examined whether this modification also facilitates rDNA release from the nucleolus. Testing the CLIP-cohibin interaction, we found that SUMO overexpression decreased Nur1 association with Lrs4 but not with its partner Heh1 (Figures 4A and S4A). We further found that SUMO overexpression results in high *ADE2* marker loss, indicating

decreased rDNA stability using USCE (Figure 4B). Notably, additional deletion of *LRS4* resulted in a non-additive phenotype, suggesting that SUMOylation and CLIP-cohibin act within the same pathway (Figure 4B). Consistently, cells expressing the SUMO isopeptidase mutant *ulp2ΔC,* which lacks the region required for Csm1 interaction (Liang et al., 2017), also showed an increased rate of marker loss (Figure S4B). When studying the location of rDNA using an mRFP-marked repeat insertion, SUMO overexpression increased the number of cells with delocalized rDNA repeats (Figure 4C), further supporting the role of SUMO in promoting rDNA release.

In contrast, transcript levels of the non-transcribed spacers NTS1 and NTS2 were not altered, indicating that the SUMO overexpression-mediated release of ribosomal repeats does not decrease rDNA silencing (Figure S4C), which is also consistent with previous reports in CLIP deficient cells (Mekhail et al., 2008). Furthermore, Csm1 association with NTS1 was not reduced, but instead enhanced under these conditions (Figure S4D). These data suggest that cohibin remains bound to rDNA after CLIP dissociation.

Since both SUMOylation and Nur1 phosphorylation stimulate CLIP-cohibin dissociation, we tested whether SUMO overexpression induces Nur1 phosphorylation. To this end, we monitored the electrophoretic mobility of Nur1 using Phos-tag gels in cells with endogenous or elevated levels of SUMO. Nur1 phosphorylation levels change in a cell-cycle-dependent manner, in agreement with previous reports (Godfrey et al., 2015), and SUMO overexpression did not affect these changes (Figure S4E). This result indicates that Nur1 phosphorylation occurs independently of SUMOylation, either upstream or in parallel. Overall, these findings argue that SUMOylation disrupts the CLIP-cohibin complex, promoting the release of ribosomal repeats.

Multiple members of the rDNA tethering complex are SUMOylated

To obtain further insights into the mechanism triggering SUMO-dependent disruption of the CLIP-cohibin complex, we used a candidate Y2H approach to identify potential SUMO substrates. Both covalent and/or non-covalent SUMO association with its targets can result in the reconstitution of the Gal4 transcription factor in Y2H assays. To distinguish between these interaction modes, we used a SUMO conjugation-deficient mutant ($SUMO^{AA}$) (Höpfler et al., 2019; Pfander et al., 2005) to test binding of partners. Using this approach, we found that all CLIP-cohibin members interact

with SUMO but not SUMO^{AA} (Figures S5A to S5C), suggesting that the rDNA tethering complex is subject to SUMOylation.

To validate these results, we examined Nur1 SUMOylation *in vivo*. Upon SUMO overexpression, Nur1 immunoprecipitation revealed an additional, slower migrating form that was further shifted when SUMO was fused to GFP (Figure 5A). These modifications were absent in cells lacking the SUMO E3 ligase Siz2 (Figure 5A). We further confirmed Nur1 SUMOylation by enriching for ^{6His}SUMO conjugates using Ni-NTA pulldowns under denaturing conditions (Figure 5B). Interestingly, SUMOylated Nur1 was also reduced in *lrs4*Δ cells and *sir2*Δ cells, or when cells were treated with nicotinamide (Figures 5B, S5D and S5E), a strong inhibitor of Sir2 activity (Bitterman et al., 2002). Together, these results imply that Nur1 is SUMOylated in a Siz2-dependent manner, and this requires CLIP association with the rDNA locus. When testing cohibin members, we failed to detect SUMOylated Lrs4 among ^{6His}SUMO conjugates using Ni-NTA pulldowns (data not shown). Therefore, we overexpressed an isopeptidase-resistant mutant of SUMO (SUMO^{Q95P}) to increase the sensitivity of SUMO conjugate detection (Pabst et al., 2019). Immunoprecipitation of Lrs4 under semi-denaturing conditions, which remove non-covalent interactions (see STAR methods), revealed an additional slower-migrating band recognized by an anti-SUMO antibody (Figure 5C). We concluded that multiple members of the CLIP-cohibin complex are SUMOylated *in vivo*.

To examine whether SUMOylation of the CLIP-cohibin complex affects rDNA stability, we determined the SUMO target sites on Nur1 by mutating putative acceptor lysine residues (K) to arginine (R). Using Ni-NTA pulldowns with ^{6His}SUMO and IP assays, we found that combined mutation of the acceptor lysine residues K175 and K176 abolished SUMOylation of Nur1 (Figures S5F and S5G). Notably, replacing Nur1 with the SUMO-deficient mutant (*nur1KR*) resulted in decreased rDNA marker loss, which was entirely dependent on the presence of Lrs4 (Figure 5D, left panel). Moreover, while *RAD52* decreases USCE as previously reported (Torres-Rosell et al., 2007), additional mutation of SUMOylation acceptor sites in Nur1 did not further reduce USCE in *rad52*Δ (Figure 5D, right panel). Overexpression of SUMO partially alleviates the USCE phenotype of *nur1KR* (Figure S5H, left). To further validate the effect of SUMO on rDNA stability, we generated strains expressing Nur1 fused to the SUMO protease domain of Ulp1 (Nur1-UD), which is expected to reduce SUMOylation of the rDNA tethering complex (Colomina

et al., 2017). Notably, the presence of Nur1-UD decreased USCE levels compared to the fusion with the catalytically dead domain of Ulp1 (Nur1-uD^{i}; Figure S5H, right). Together, this argues that Nur1 SUMOylation acts upstream of Rad52-mediated recombination, and that increased SUMOylation of other CLIP-cohibin members can compensate for the loss of Nur1 SUMOylation.

To validate the role of SUMOylation in the rDNA tethering complex through a gain-of-function approach, we expressed Nur1 and Lrs4 as linear fusions with SUMO in *nur1*Δ and *lrs4*Δ cells, respectively, and examined rDNA stability by USCE. Notably, while expressing non-fused Nur1 and Lrs4 rescued the deletion mutants, the SUMO fusion proteins failed to complement the USCE phenotype (Figure 5E). Several proteins have been shown to interact with SUMO with moderate affinity through their SIMs (Geiss-Friedlander and Melchior, 2007). We therefore introduced mutations into the SUMO moiety preventing its recognition by SIMs (SUMO^{FAIA}) in the linear Nur1 and Lsr4 SUMO fusion proteins (Newman et al., 2017). When assessing rDNA recombination, these SUMO^{FAIA} fusions displayed USCE rates that are significantly lower than the corresponding WT-SUMO fusions, and comparable to the non-fusion proteins (Figure 5E). This implies that the specific recognition of SUMO in the rDNA tethering complex triggers rDNA recombination. In agreement with this observation, we found that the Lrs4 interaction with CLIP is strongly reduced when WT SUMO is overexpressed, but not the SIM mutant (Figure 5F). These data argue that SUMOylation on CLIP-cohibin, likely through SUMO-dependent recruitment of other protein(s), promotes rDNA relocation.

Cdc48 recognizes the CLIP-cohibin complex and supports rDNA release

The AAA-ATPase Cdc48 (also known as VCP/p97) acts as a segregase to disassemble protein complexes during proteasomal degradation, but also has functions in non-proteolytic pathways, such as DNA damage repair (Franz et al., 2016). Besides recognizing ubiquitylated proteins, Cdc48 has also been reported to bind to SUMOylated proteins (Bergink et al., 2013; Nie et al., 2012). Therefore, we tested whether the CLIP-cohibin complex is targeted by Cdc48 in a SUMO-dependent manner. We found that Cdc48 interacts weakly with Lrs4 in WT cells using coIP. This interaction was increased in cells overexpressing either a thermosensitive allele (*cdc48-6*) or an ATPase deficient mutant (*cdc48 E588Q*; Figure 6A), known to block or delay the release of substrates, respectively (Bergink

et al., 2013; Bodnar and Rapoport, 2017). We also observed increased Cdc48 interaction with Nur1 in *cdc48-6* cells (Figure 6B). When examining the CLIP-cohibin association, Lrs4 binding to Nur1 was modestly increased in *cdc48-6* or *cdc48 E588Q* cells (Figure 6C). Together, these results suggest that Cdc48 assists in the disruption of the rDNA tethering complex.

Cdc48 recognize SUMOylated proteins through its substrate-recruiting cofactor Ufd1 that contains a SIM motif (Figure 6D) (Bergink et al., 2013; Nie et al., 2012). Consistent with this, we found that both Lrs4 and Nur1 interact with Ufd1 in Y2H assays, and this interaction is SIM-dependent (Figures 6E and 6F). Notably, *ufd1*Δ*SIM* cells displayed a significant reduction of USCE, suggesting that recognition of SUMOylated Nur1 or Lrs4 is critical for rDNA release and recombination. In agreement with this notion, the decrease in USCE in *ufd1*Δ*SIM* mutant cells was completely relieved when Lrs4 was absent (Figures 6G, left panel). Furthermore, SUMO overexpression did not significantly alter the USCE phenotype of *ufd1*Δ*SIM* cells (Figure 6G, right panel), implying that Ufd1 acts downstream of SUMOylation in the maintenance of rDNA stability. We further tested the role of STUbLs, which have been reported to contribute to rDNA stability and recruit Cdc48 in a SUMO-dependent manner (Cal-Bkowska et al., 2011; Gillies et al., 2016; Liang et al., 2017). However, deletion of the STUbLs *SLX5*, *SLX8* or *ULS1* did not affect CLIP-cohibin association (Figures S6A and S6B). Together, these results suggest that Cdc48 recognizes the CLIP-cohibin complex, and promotes rDNA relocation in a SUMO- and Ufd1-dependent manner.

While our findings suggested that Nur1 phosphorylation does not depend on SUMOylation, both modifications may contribute to rDNA release through the same pathway, with SUMOylation/Cdc48 acting downstream of Nur1 phosphorylation. We thus assessed USCE in cells deficient in Nur1 phosphorylation (*nur1Pmut*), SUMO recognition by Ufd1 (*ufd1*Δ*SIM*), or the combination of both. While *ufd1*Δ*SIM* cells displayed lower USCE rates than *nur1Pmut*, the double mutant displayed a non-additive phenotype (Figure 6H), suggesting that both modifications affect the same pathway.

DNA damage triggers the dissociation of the rDNA tethering complex

DNA damage repair requires nuclear membrane release prior to the relocation of the rDNA repeats. To examine whether CLIP-cohibin disassembly plays a role in this

physiological context, we studied its association and modification in response to double-strand breaks (DSBs). To this end, we transiently expressed the *Physarum polycephalum* homing endonuclease I-*Ppo*I, which generates DSBs at every rDNA repeat (Monnat et al., 1999; Muscarella and Vogt, 1993), from the galactose-inducible strong *GAL1* and moderate *GALL* promoters. Quantitative PCR analysis of genomic DNA confirmed that I-*Ppo*I expression induces DSBs within rDNA repeats in a dose-dependent manner without affecting the rDNA copy number (Figures 7A and 7B). When studying CLIP association with cohibin by coIP, we found that Heh1 binding to Lrs4 was reduced upon I-*Ppo*I induction (Figure 7A), whereas Lrs4 association with rDNA was not altered (Figure 7B), suggesting that rDNA breaks trigger CLIP-cohibin disassembly. In agreement with this finding, we observed that I-*Ppo*I induction increases Nur1 phosphorylation (Figure S7A) and the appearance of global SUMO conjugates (Figure S7B). To investigate whether preventing CLIP-cohibin disassembly affects rDNA release after damage, we performed live-cell imaging to monitor the nucleolar location of a *tetO*/TetI^{mRFP}-marked repeat flanked by an I-*Sce*I endonuclease cut site. After I-*Sce*I induction, generation of a single DSB caused rDNA relocation to an extranucleolar site (Figure 7C), as previously reported (Torres-Rosell et al., 2007). Notably, rDNA relocation was substantially reduced in a *ufd1*Δ*SIM* mutant, which impairs SUMO recognition by Cdc48 and likely acts downstream of CLIP and cohibin SUMOylation (Figure 7C). Based on these results, we conclude that DSBs at the rDNA repeats promote nucleolar release through controlled disassembly of the tethering complex through Nur1 phosphorylation and SUMO-dependent Cdc48 activity.

UFD1 promotes rDNA release in human cells upon DNA damage

Since relocation of ribosomal repeats during DNA damage repair is a conserved mechanism (Harding et al., 2015; van Sluis and McStay, 2015), we speculated that key processes regulating rDNA dynamics might also be present in humans. To test this, we examined rDNA release upon damage in RPE (retinal pigment epithelium) cells depleted of the Ufd1 homolog, UFD1L. To generate DSBs in rDNA repeats, we used a tetracyclin-inducible expression system consisting of I-*Ppo*I fused to the FKBP12 destabilization domain, which can be stabilized by the addition of the compound shield-1 (Warmerdam et al., 2016). The movement of damaged repeats outside the nucleolus was assessed by quantifying the location of γH2AX foci, a

marker for damaged DNA sites, relative to the nucleolar marker nucleophosmin (NPM). As previously reported, broken repeats were released to a large extent from the nucleolus of control cells upon expression of I-*Ppo*I, as calculated by the number of cells with γH2AX foci within the nucleolus (Figures 7D and 7E) (Harding et al., 2015; van Sluis and McStay, 2015; Warmerdam et al., 2016). Upon depletion of UFD1L, we found that nucleolar segregation was reduced by more than 50% after damage relative to inhibition of the DNA damage checkpoint kinase ATM (ataxia telangiectasia-mutated), which resulted in a complete block of nucleolar release (Figures 7D, 7E and S7C). In contrast to yeast, the interaction between p97 and SUMO has not been described in humans. However, p97 is targeted to SUMOylated substrates with the aid of the STUbL RNF4 (Franz et al., 2016; Gibbs-Seymour et al., 2015; Sun et al., 2007). Notably, depletion of RNF4 blocks rDNA relocation upon damage, and additional UFD1L knock-down resulted in a non-additive phenotype, suggesting that RNF4 and p97 together assist relocation away from the nucleolus (Figure 7E). These results suggest that the role of Cdc48/p97 in controlling rDNA release during rDNA damage repair is conserved from yeast to humans.

Discussion

The nucleolus shields the rDNA locus from uncontrolled recombination in eukaryotes, but this requires relocation to the nucleoplasm should DNA damage repair be needed (van Sluis and McStay, 2015; Torres-Rosell et al., 2007). However, how individual rDNA repeats exit the nucleolus was previously poorly understood. Here, we have identified the critical steps triggering the nucleolar release of rDNA repeats in yeast both under normal growth conditions and after exogenous DNA damage. These molecular events include Nur1 phosphorylation (Figure 3), which accumulates upon DSB formation in rDNA repeats (Figure S7). The effects of Nur1 phosphorylation are counteracted by the phosphatase Cdc14. It further requires Siz2-dependent SUMOylation of Nur1 and Lrs4, which earmarks the rDNA tethering complex for disassembly and likely occurs downstream of Nur1 phosphorylation (Figure 5). Repeat release from the membrane-bound CLIP complex is ultimately mediated by the AAA-ATPase Cdc48/p97 in conjunction with its cofactor Ufd1 through recognition of SUMOylated Nur1 and Lrs4, which allows rDNA relocation and repair by Rad52 (Figure 6 and 7).

The segregase Cdc48/p97 plays a key role in many cellular processes, including the DNA damage response, where it segregates ubiquitylated proteins from non-modified partner proteins to facilitate their proteasomal degradation. Recognition of ubiquitylated proteins is mediated by the heterodimeric cofactor Ufd1-Npl4, whereas other co-factors help Cdc48 to orchestrate the delivery to the proteosome (Franz et al., 2016). However, several studies revealed that Cdc48 also participates in disassembling protein complexes marked with SUMO (Bergink et al., 2013; Mérai et al., 2014; Nie et al., 2012). Consistent with these reports, we discovered that Cdc48 binds to SUMOylated Nur1 and Lrs4 through Ufd1 and disrupts the CLIP-cohibin complex to promote rDNA relocation upon damage (Figures 6 and 7). Presenting multiple SUMOylated substrates may increase the efficiency of $Cdc48^{Ufd1\text{-}Npl4}$-mediated CLIP-cohibin disassembly, and in agreement we found that overexpressing SUMO compensates for deficient rDNA recombination in the *nur1KR* mutant (Figure S5). Additionally, we found that depletion of the p97 cofactor UFD1L impairs the nucleolar segregation of broken rDNA repeats in human cells (Figure 7). This implies that the role of $Cdc48/p97^{Ufd1\text{-}Npl4}$ in rDNA release is conserved between yeast and humans, although the human substrate(s) remain(s) to be identified. Given the presence of mixed SUMO-ubiquitin chains, generated by STUbL E3 ligases, it has

been proposed that Cdc48 can be recruited to its targets by a dual mechanism (Franz et al., 2016; Nie et al., 2012). Besides recognizing SUMOylated proteins, Ufd1 has been reported to bind directly to the fission yeast STUbL Rfp1 (homologous to *S. cerevisiae* Slx5/8 and human RNF4) (Køhler et al., 2013). We found that deletion of the STUbLs Slx5, Slx8 or Uls1 did not affect CLIP-cohibin dissociation (Figure S6). However, we cannot exclude the possibility that STUbLs are involved downstream of CLIP-cohibin disassembly. It is thus noteworthy that the STUbL RNF4 acts together with UFD1L to release rDNA from the nucleolus upon damage (Figure 7), implying a functional link between ubiquitylation and p97 in relocating rDNA in human cells.

In addition to SUMO modification, Nur1 phosphorylation is another critical step controlling rDNA release (Figures 3, S4 and 6). Nur1 is phosphorylated by the cyclin-dependent kinase Cdk1 to attenuate the release of the phosphatase Cdc14 during the cell cycle, which removes the modification in late anaphase (Godfrey et al., 2015; Holt et al., 2009). We found that Nur1 phosphorylation is also induced in response to DSBs (Figure S7A). While CDK is inhibited after DNA damage in metazoans (Lanz et al., 2019), yeast Cdk1 was previously reported to be active at DSBs (Bantele et al., 2017; Huertas et al., 2008; Ira et al., 2004). It is therefore possible that this kinase is also involved in Nur1 phosphorylation during rDNA damage. Furthermore, cell cycle-dependent Nur1 phosphorylation might also serve as a signal to release the rDNA locus from the nuclear envelope to allow chromosome segregation, which would be counteracted by Cdc14 activity at the end of mitosis (Dauban et al., 2019; Godfrey et al., 2015). Alternatively, Nur1 could also be modified by DNA damage checkpoint kinases. For instance, ATM-mediated phosphorylation of Treacle (also known as *TCOF1*) is required to modulate the nucleolar response during rDNA damage in humans (Korsholm et al., 2019; Mooser et al., 2020). The molecular mechanism by which Nur1 phosphorylation triggers CLIP-cohibin disruption remains unknown. While SUMOylation does not affect Nur1 phosphorylation (Figure S4), both appear to act in the same pathway (Figure 6), suggesting that Nur1 phosphorylation occurs upstream, and presumably controls SUMOylation. Consistent with this model, phosphorylation of other targets are known to stimulate their SUMOylation (Hietakangas et al., 2006; Kang et al., 2006).

Maintaining dynamic regulation of the CLIP-cohibin complex appears to be critical, since we find that tethering rDNA repeats permanently to the nuclear envelope is

lethal (Figure 1). We propose that this is likely due to the failure to repair broken repeats, as the rDNA has been reported to be frequently damaged and relocated even in the absence of exogenous DNA damage (Torres-Rosell et al., 2007). However, we cannot exclude the possibility that permanent rDNA tethering also affects rDNA release during mitosis. Indeed, release of the *S. japonicus* CLIP complex from centromeres and telomeres is crucial for proper progression of mitosis (Pieper et al., 2020). Nonetheless, perinuclear anchoring of other genomic loci does not affect cell survival. For instance, artificial tethering of the mating-type loci in *S. cerevisiae* enhances transcriptional silencing without affecting cell growth (Andrulis et al., 1998). In agreement, we found that permanent perinuclear tethering of genomic regions recognized by the Gal4 transcription factor allowed normal growth (Figure 1). Together, these data suggest that maintaining a dynamic spatial regulation is specifically important for repetitive sequences, but independent of perinuclear release during mitosis in general.

In conclusion, we favor a model where phosphorylation and SUMOylation of the rDNA tethering complex act together to promote complex dissociation and modulate the release of broken repeats to be repaired (Figure 7E). Remarkably, the spatial control of damaged rDNA repeats is highly reminiscent of other repair pathways, specifically the repair of DSBs within pericentromeric heterochromatin in flies and mice (Chiolo et al., 2011; Tsouroula et al., 2016). In this case HR progression is temporally blocked by SUMO and the Smc5/6 complex, whereas SUMOylation and ubiquitylation by STUbLs promotes the relocation of the damaged locus outside heterochromatin, and its targeting to the nuclear periphery for DNA damage repair (Chiolo et al., 2011; Ryu et al., 2015; Tsouroula et al., 2016). Our results provide another example of how cells utilize similar molecular mechanisms to control the relocation of repetitive sequences and thus maintain genome integrity.

Materials and Methods

Yeast strains

Yeast strains isogenic to W303 or DF5 were used for genetic studies, and PJ69-7a, Y187 or Y2H Gold for yeast two-hybrid assays.

Yeast methods and molecular biology

Standard protocols for transformation, mating, sporulation and tetrad dissection were used for yeast manipulations (Sherman, 2002). Unless indicated otherwise, cells were grown at 30˚C in YPD medium (1% yeast extract, 2% peptone and 2% glucose) or synthetic complete medium lacking individual amino acids to maintain selection for transformed plasmids. Protein tagging and the construction of deletion mutants were conducted by a PCR-based strategy and confirmed by immunoblotting and PCR, respectively (Janke et al., 2004; Knop et al., 1999). For galactose induction, cells were cultured in medium supplemented with 2% raffinose, and galactose was added to a mid-log phase yeast cells to a final concentration of 2%. For Nur1 C-terminal tagging with the active or inactive catalytic domain of SUMO-protease Ulp1 were performed using the pYM15-UD and pYM-uD^{i}, respectively (Colomina et al., 2017). For auxin-inducible degradation, cells expressing the protein of interest fused to an auxin-dependent degron sequence derived from IAA17 together with the F-box protein TIR1 from *Oriza sativa* were cultured in YPD medium until mid-log phase, and the synthetic auxin analog 1-naphthaleneacetic acid (NAA) was added to a final concentration of 1.5 mM for 2h (Morawska and Ulrich, 2013). Damage in rDNA repeats using I-*Ppo*I fused to the mouse glucocorticoid receptor was induced by adding galactose and triamcinolone acetonide to a final concentration of 2% and 7.5 µM or 75 µM, respectively, to a mid-log phase yeast cells growing in minimal selective media with 2% raffinose for 3h (Wright et al., 1990). Yeast growth assays were performed by spotting five-fold serial dilutions of the indicated strains on solid agar plates.

Cloning methods used standard protocols or the Gibson Assembly Master Mix (NEB). For yeast two-hybrid experiments, the different constructs were cloned into *pGADT7* or *pGBKT7* vectors (Clontech™). Plasmids with point mutations or deletions were constructed by the PCR-based site-directed mutagenesis approach. Maps DNA sequences are available upon request.

Live-cell imaging and analysis

For fluorescence microscopy, cells were diluted to OD_{600}=0.15 in synthetic complete medium lacking individual amino acids, and grown until OD_{600}=0.8-1.2 before imaging. Microscopy slides (MatTek) were pretreated with 1 mg ml^{-1} concanavalin A solution. Imaging was performed on a Zeiss AxioObserver Z1 confocal spinning-disk microscope equipped with an Evolve 512 (Photometrics) EMM-CCD camera through a Zeiss Alpha Plan/Apo 100×/1.46 oil DIC M27 objective lens. Optical section images were obtained at focus intervals of 0.2 µm. Subsequent processing and analyses of the images were performed in Fiji/ImageJ (Schindelin et al., 2012). For induction of I-*Sce*I endonuclease (rDNA damage), cells were grown at 30˚C in synthetic complete medium lacking individual amino acids plus 2% raffinose to an OD_{600}=0.6 and expression of I-*Sce*I was induced by addition of 2% galactose for 2h.

Unequal sister chromatid exchange assays

Assays were performed as previously described (Huang et al., 2006), with some modifications. Cells were grown in YPDA or synthetic complete medium lacking individual amino acids to OD_{600}=0.8-1.2, diluted 1:1,000 in distilled H_2O and plated on synthetic complete medium plates. Cells were incubated at 30˚C (for 3 days in glucose-containing medium, or for 4 days in galactose-containing medium) and then transferred to 4˚C for 3 days to enhance color development. The rate of marker loss was calculated by dividing the number of half-red/half-white colonies by the total number of colonies. Red colonies were excluded from all calculations.

Immunoblotting

Total protein extracts from $2x10^7$ cells (OD_{600}=1) were prepared by trichloroacetic acid (TCA) precipitation (Knop et al., 1999). Proteins solubilized in HU loading buffer (8 M urea, 5% SDS, 200 mM Tris-HCl pH 6.8, 20 mM dithiothreitol (DTT) and bromophenol blue 1.5 mM) were resolved on NuPAGE 4%-12% gradient gels (Invitrogen), transferred onto polyvinylidene fluoride membranes (Immobilon-P) and analyzed by standard immunoblotting techniques using specific antibodies (see the 'Antibodies' section).

Co-immunoprecipitation

Cell lysates were prepared by resuspending the pellets from 150-200 OD_{600} units in 800 µl lysis buffer (50 mM Tris pH 7.5, 150 mM NaCl, 10% glycerol, 1 mM EDTA pH 8, 0.5% NP-40, 1x complete EDTA-free protease inhibitor cocktail (Roche), 2 mM PMSF, 20 mM N-ethylmaleimide (NEM)). To block phosphatase activity, 1x tablet of PhosSTOP, 10 mM NaF and 20 mM ß-glycerophosphate were added to the lysis buffer. Cells were lysed by bead-beating (Precellys 24, Bertin instruments) with zirconia/silica beads (BioSpec Inc.) and lysates were cleared by centrifugation (800g, 5 min). Clarified extracts were incubated with pre-equilibrated antiHA-sepharose (Roche), GFP-Trap (Chromotek) or IgG-agarose beads (Sigma) for 1.5 hours at 4˚C, beads were washed four times with lysis buffer and two times with wash buffer (50 mM Tris pH 7.5, 150 mM NaCl, 1 mM EDTA pH 8). Proteins were eluted by boiling with 30 µl HU loading buffer and analyzed by immunoblotting.

Analysis of protein SUMOylation using semi-denaturing purification

To examine SUMOylated GFP-tagged proteins, cell lysates from 200 OD_{600} units from cells with or without rDNA damage were prepared as for co-immunoprecipitation experiments. Clarified extracts were incubated with 12.5 µl pre-equilibrated GFP-Trap beads (Chromotek) for 1.5 hours at 4˚C, beads were washed once with lysis buffer. As reported for the detection of other post-translational modifications (Juretschke et al., 2019), the GFP-Trap beads were then washed five times with denaturation buffer (PBS, 8 M urea). The specifically bound proteins were eluted by boiling with 30 µl HU loading buffer and analyzed by immunoblotting.

Analysis of protein SUMOylation by Ni-NTA pulldowns

To detect proteins covalently modified with SUMO, 200 OD_{600} units from cells expressing N-terminally histidine-tagged SUMO (6 histidines) under the control of the ADH1 promoter, integrated at the *URA3* locus, were collected. Subsequently, Ni-NTA pulldowns using Ni-NTA magnetic agarose beads (Qiagen) were performed as previously described (Psakhye and Jentsch, 2016).

Chromatin immunoprecipitation (ChIP)

ChIP experiments were performed as described previously (Braun et al., 2011), with some modifications. Briefly, 150 ml cell cultures were grown to OD_{600}=0.8-1.0, cross-

linked (1% formaldehyde, 16 min, room temperature) and lysed by bead beating. The chromatin fraction was isolated and sheared to 200bp - 500bp fragments (30 min, 30-sec on/off cycles, 90% amplitude) using a Q800R1 sonicator (QSonica). Immunoprecipitations were performed overnight at 4˚C with 100 µl of 25% slurry of prewashed IgG-agarose beads (Sigma) from lysates corresponding to 80-100 OD_{600} of cells. The beads were washed and eluted, and the eluate was reverse cross-linked at 65˚C for 3 h and incubated with proteinase K for 2 h at 55˚C. DNA was cleaned up with ChIP DNA Clean & Concentrator™ kit (#D5201, Zymo Research). Immunoprecipitated DNA was quantified by qPCR using primaQUANT SYBR Master mix (Steinbrenner Laborsysteme GmbH. #SL-9902B) and a QuantStudio™ 3/5 Real-Time PCR system (Applied Biosystems/Thermo Fisher). Primers are listed in Table S1. To avoid changes due to different rDNA copy number, the relative fold enrichment for each strain was determined over the average of three rDNA positions (RDN1 #9, RDN1 #12 and RDN1 #25), after normalization to input: [rDNA(IP)/rDNA(WCE)]/[mean(rDNA)(IP)/mean(rDNA)(WCE)].

Determination of rDNA copy number and induction of double-strand breaks

The amount of cells corresponding to OD_{600}=1 ($2x10^7$ cells) was harvested before and after induction of rDNA damage using I-*Ppo*I (uninduced and induced samples, respectively), and genomic DNA was prepared using the MasterPure Yeast DNA Purification Kit (Epicenter). Genomic DNA was then used as input for qPCR with specific primers (Table S1). The relative rDNA copy number or intact I-*Ppo*I cut site (rDNA damage efficiency) was calculated as the ratio between induced and uninduced samples, after normalized to a control locus on chromosome VI (*ACT1*).

Quantitative RT-qPCR

RT-qPCR analyses were performed as previously described (Braun et al., 2011). cDNAs were quantified by qPCR using primaQUANT SYBR Master mix (Steinbrenner Laborsysteme GmbH) and a QuantStudioTM 3 Real-Time PCR system (Applied Biosystems/Thermo Fisher). Primers are listed in Table S1. For the calculation of mean values and standard deviation from independent experiments, *ACT1*-normalized data sets are shown in log_2 scale as relative to the mean value of the wild type.

Cell culture

RPE cells were grown in DMEM (Sigma) supplemented with Penicillin-Streptomycin (Life Technologies), L-Glutamine (ThermoFisher) and 10% fetal bovine serum (FBS) (Takarabio) at 37˚C and 5% CO_2. RNAi experiments were performed using RNAiMax (Life Technologies) two days before treatments. The following siRNA sequences were used: siControl (5'-UGGUUUACAUGUCGACUAA-3'; Metabion), siUFD1La (5'-GUGGCCACCUACUCCAAAUUU-3'; Metabion), siUFD1Lb (5'-CUACAAAGAACCCGAAAGAUUUU-3'; Metabion). I-*Ppo*I expression was induced by adding doxycycline (1 µg/ml, Sigma) 4h and Shield-1 (1 µM, Aobious) 1h before fixation.

Immunofluorescence

Cells were washed with PBS (Sigma) and fixed in 4% paraformaldehyde for 30 min at room temperature. Then, cells were permeabilized in CSK buffer (10 mM HEPES pH 7.4, 300 mM Sucrose, 100 mM NaCl, 3 mM $MgCl_2$) with 0.1% Triton-X for 30 min. Blocking was performed for 1 h with 5% FBS in PBS after which cells were stained in 1% FBS in PBS overnight at 4˚C. After primary staining, cells were washed 3 times 5 min with PBS and incubated with secondary antibodies for 1h at RT. After another three 5 min washes in PBS, slides were mounted with Aqua-Poly/Mount (Polysciences). Images were obtained using an AxioObserver Z1 confocal spinning-disk microscope (Zeiss) equipped with an AxioCam HRm CCD camera (Zeiss) or a sCMOS ORCA Flash 4.0 camera (Hamamatsu) and a Plan/Apo 63 Å~/1.4 water-immersion objective. Blinded visual scoring of rDNA damage retention was performed by two individuals.

Antibodies

Polyclonal Smt3 (1:5,000) and Cdc48 (1:5,000) antibodies were raised in rabbits and have been described previously (Hoege et al., 2002; Richly et al., 2005). Monoclonal antibodies directed against the HA epitope (1:1,000; 3F10) and monoclonal antibody against GFP (1:1,000; B-2) were purchased from Roche and Santa Cruz Biotechnology, respectively. Mouse monoclonal antibodies against Dpm1 (1:2,000; 5C5A7) and Pgk1 (1:5,000; 22C5D8) were obtained from Invitrogen. Mouse monoclonal antibodies against phospho-H2AX (Ser139) (1:1,000, JBW301) were

obtained from Merck Millipore. Rabbit polyclonal antibodies against Nucleophosmin (1:100, ab15440) and Rad53 (1:1000, ab104232) were purchased from Abcam. Secondary antibodies goat-α-mouse IgG Alexa fluor 488 (1:5,000; A11001) and donkey-α-rabbit IgG Alexa fluor 568 (1:5,000; A10042) were obtained from Thermo Fisher Scientific.

Statistics and reproducibility

Representative results of at least two independent experiments were presented in all of the figure panels. Analyses of the variance (ANOVA) were performed, and pairwise differences were evaluated with Tukey's *post hoc* test using R statistical language (R Development Core Team, 2008); different groups are marked with letters at the 0.05 significance level. For all error bars, data are mean ± S.E.M. P values for all graphs were generated using two-tailed Student's t-tests; N/S, $P \geq 0.05$, $^{*}P \leq 0.05$, $^{**}P \leq 0.01$, $^{***}P \leq 0.001$.

Acknowledgements

We thank members of the Braun and Ladurner labs for fruitful discussions and critical comments on the manuscript; R. H. Medema for RPE cell lines; Dr. J. Torres-Rosell for *pYM15-UD* and *pYM15-uD*^{i} plasmids; Dr. F. den Brave for pCu415 plasmids; P. Bourilhon and D. Sinitski for mouse cDNA and reagents; S. Fischer-Burkart, T. S. van Emden and A. Muhammad for assistance, especially during COVID-19 times. This work was supported by a grant awarded to SB from the German Research Foundation (DFG; BR 3511/4-1). IKM is recipient of a grant from the Stiftungskommission of the LMU Medical Faculty. Research in the SJ laboratory was supported by Max Planck Society (MPG), Center for Integrated Protein Science Munich (CIPSM), Louis-Jeantet Foundation, and a European Research Council (ERC) Advanced Grant. Research in the SB, BP, and AGL laboratories was further supported by the DFG through the collaborative research center CRC 1064 (project ID 213249687-SFB 1064), LMU (AGL) and MPG (BP).

Author contributions

MC, SJ and SB conceived the study. IKM performed the mammalian experiments, and LMC contributed to the microscopy studies using yeast. MC performed all other experiments. MC, IKM, and LMC analyzed the data. SB, SJ and BP supervised the project. SB, SJ and AGL acquired funding. MC and SB conceived and wrote the manuscript, and all authors contributed to editing.

Declaration of interests

The authors declare no competing interests.

References

Andrulis, E.D., Neiman, A.M., Zappulla, D.C., and Sternglanz, R. (1998). Perinuclear localization of chromatin facilitates transcriptional silencing. Nature *394*, 592–595.

Bantele, S.C.S., Ferreira, P., Gritenaite, D., Boos, D., and Pfander, B. (2017). Targeting of the Fun30 nucleosome remodeller by the Dpb11 scaffold facilitates cell cycle-regulated DNA end resection. Elife *6*, 1–21.

Bergink, S., Ammon, T., Kern, M., Schermelleh, L., Leonhardt, H., and Jentsch, S. (2013). Role of Cdc48/p97 as a SUMO-targeted segregase curbing Rad51-Rad52 interaction. Nat. Cell Biol. *15*, 526–532.

Bitterman, K.J., Anderson, R.M., Cohen, H.Y., Latorre-Esteves, M., and Sinclair, D.A. (2002). Inhibition of silencing and accelerated aging by nicotinamide, a putative negative regulator of yeast Sir2 and human SIRT1. J. Biol. Chem. *277*, 45099–45107.

Bodnar, N.O., and Rapoport, T.A. (2017). Molecular Mechanism of Substrate Processing by the Cdc48 ATPase Complex. Cell *169*, 722-735.e9.

Braun, S., Garcia, J.F., Rowley, M., Rougemaille, M., Shankar, S., and Madhani, H.D. (2011). The Cul4-Ddb1Cdt2 ubiquitin ligase inhibits invasion of a boundary-associated antisilencing factor into heterochromatin. Cell *144*, 41–54.

Cal-Bkowska, M., Litwin, I., Bocer, T., Wysocki, R., and Dziadkowiec, D. (2011). The Swi2-Snf2-like protein Uls1 is involved in replication stress response. Nucleic Acids Res. *39*, 8765–8777.

Capella, M., Caballero, L.M., Pfander, B., Braun, S., and Jentsch, S. (2020). ESCRT recruitment by the inner nuclear membrane protein Heh1 is regulated by Hub1-mediated alternative splicing. J. Cell Sci. jcs.250688.

Chiolo, I., Minoda, A., Colmenares, S.U., Polyzos, A., Costes, S. V., and Karpen, G.H. (2011). Double-strand breaks in heterochromatin move outside of a dynamic HP1a domain to complete recombinational repair. Cell *144*, 732–744.

Churikov, D., Charifi, F., Eckert-Boulet, N., Silva, S., Simon, M.N., Lisby, M., and Géli, V. (2016). SUMO-Dependent Relocalization of Eroded Telomeres to Nuclear Pore Complexes Controls Telomere Recombination. Cell Rep. *15*, 1242–1253.

Colomina, N., Guasch, C., and Torres-Rosell, J. (2017). Analysis of SUMOylation in the RENT complex by fusion to a SUMO-specific protease domain. Methods Mol. Biol. *1505*, 97–117.

Corbett, K.D., Yip, C.K., Ee, L.S., Walz, T., Amon, A., and Harrison, S.C. (2010). The monopolin complex crosslinks kinetochore components to regulate chromosome-microtubule attachments. Cell *142*, 556–567.

Dauban, L., Kamgoué, A., Wang, R., Léger-Silvestre, I., Beckouët, F., Cantaloube, S., and Gadal, O. (2019). Quantification of the dynamic behaviour of ribosomal DNA genes and nucleolus during yeast Saccharomyces cerevisiae cell cycle. J. Struct. Biol. *208*, 152–164.

Franz, A., Ackermann, L., and Hoppe, T. (2016). Ring of change: CDC48/p97 drives protein dynamics at chromatin. Front. Genet. *7*, 1–14.

Geiss-Friedlander, R., and Melchior, F. (2007). Concepts in sumoylation: A decade on. Nat. Rev. Mol. Cell Biol. *8*, 947–956.

Gibbs-Seymour, I., Oka, Y., Rajendra, E., Weinert, B.T., Passmore, L.A., Patel, K.J., Olsen, J. V., Choudhary, C., Bekker-Jensen, S., and Mailand, N. (2015). Ubiquitin-SUMO circuitry controls activated fanconi anemia ID complex dosage in response to DNA damage. Mol. Cell *57*, 150–164.

Gillies, J., Hickey, C.M., Su, D., Wu, Z., Peng, J., and Hochstrasser, M. (2016). SUMO pathway modulation of regulatory protein binding at the ribosomal dna locus in Saccharomyces cerevisiae. Genetics *202*, 1377–1394.

Godfrey, M., Kuilman, T., and Uhlmann, F. (2015). Nur1 Dephosphorylation Confers Positive Feedback to Mitotic Exit Phosphatase Activation in Budding Yeast. PLoS Genet. *11*.

Grund, S.E., Fischer, T., Cabal, G.G., Antúnez, O., Pérez-Ortín, J.E., and Hurt, E. (2008). The inner nuclear membrane protein Src1 associates with subtelomeric genes and alters their regulated gene expression. J. Cell Biol. *182*, 897–910.

Hallgren, J., Pietrzak, M., Rempala, G., Nelson, P.T., and Hetman, M. (2014). Neurodegeneration-associated instability of ribosomal DNA. Biochim. Biophys. Acta - Mol. Basis Dis. *1842*, 860–868.

Harding, S.M., Boiarsky, J.A., and Greenberg, R.A. (2015). ATM Dependent Silencing Links Nucleolar Chromatin Reorganization to DNA Damage Recognition. Cell Rep. *13*, 251–259.

Hietakangas, V., Anckar, J., Blomster, H.A., Fujimoto, M., Palvimo, J.J., Nakai, A., and Sistonen, L. (2006). PDSM, a motif for phosphorylation-dependent SUMO modification. Proc. Natl. Acad. Sci. U. S. A. *103*, 45–50.

Hoege, C., Pfander, B., Moldovan, G.L., Pyrowolakis, G., and Jentsch, S. (2002). RAD6-dependent DNA repair is linked to modification of PCNA by ubiquitin and SUMO. Nature *419*, 135–141.

Holt, L.J., Tuch, B.B., Villen, J., Johnson, A.D., Gygi, S.P., and Morgan, D.O. (2009). Global analysis of cdk1 substrate phosphorylation sites provides insiqhts into evolution. Science (80-.). *325*, 1682–1686.

Höpfler, M., Kern, M.J., Straub, T., Prytuliak, R., Habermann, B.H., Pfander, B., and Jentsch, S. (2019). Slx5/Slx8-dependent ubiquitin hotspots on chromatin contribute to stress tolerance. EMBO J. *38*, 1–19.

Horigome, C., and Gasser, S.M. (2016). SUMO wrestles breaks to the nuclear ring's edge. Cell Cycle *15*, 3011–3013.

Horigome, C., Bustard, D.E., Marcomini, I., Delgoshaie, N., Tsai-Pflugfelder, M., Cobb, J.A., and Gasser, S.M. (2016). PolySUMOylation by Siz2 and Mms21 triggers relocation of DNA breaks to nuclear pores through the Slx5/Slx8 STUbL. Genes Dev. *30*, 931–945.

Huang, J., Brito, I.L., Villén, J., Gygi, S.P., Amon, A., and Moazed, D. (2006). Inhibition of homologous recombination by a cohesin-associated clamp complex recruited to the rDNA recombination enhancer. Genes Dev. *20*, 2887–2901.

Huertas, P., Cortés-Ledesma, F., Sartori, A.A., Aguilera, A., and Jackson, S.P. (2008). CDK targets Sae2 to control DNA-end resection and homologous recombination. Nature *455*, 689–692.

Ira, G., Pellicioll, A., Balijja, A., Wang, X., Florani, S., Carotenuto, W., Liberi, G., Bressan, D., Wan, L., Hollingsworth, N.M., et al. (2004). DNA end resection, homologous recombination and DNA damage checkpoint activation require CDK1. Nature *431*, 1011–1017.

Jaco, I., Canela, A., Vera, E., and Blasco, M.A. (2008). Centromere mitotic recombination in

mammalian cells. J. Cell Biol. *181*, 885–892.

Jalal, D., Chalissery, J., and Hassan, A.H. (2017). Genome maintenance in Saccharomyces cerevisiae: The role of SUMO and SUMO-targeted ubiquitin ligases. Nucleic Acids Res. *45*, 2242–2261.

Janke, C., Magiera, M.M., Rathfelder, N., Taxis, C., Reber, S., Maekawa, H., Moreno-Borchart, A., Doenges, G., Schwob, E., Schiebel, E., et al. (2004). A versatile toolbox for PCR-based tagging of yeast genes: New fluorescent proteins, more markers and promoter substitution cassettes. Yeast *21*, 947–962.

Johzuka, K., and Horiuchi, T. (2009). The cis Element and Factors Required for Condensin Recruitment to Chromosomes. Mol. Cell *34*, 26–35.

Juretschke, T., Beli, P., and Dikic, I. (2019). Quantitative phosphoproteomics of selective autophagy receptors. Methods Mol. Biol. *1880*, 691–701.

Kalocsay, M., Hiller, N.J., and Jentsch, S. (2009). Chromosome-wide Rad51 Spreading and SUMO-H2A.Z-Dependent Chromosome Fixation in Response to a Persistent DNA Double-Strand Break. Mol. Cell *33*, 335–343.

Kang, J., Gocke, C.B., and Yu, H. (2006). Phosphorylation-facilitated sumoylation of MEF2C negatively regulates its transcriptional activity. BMC Biochem. *7*, 1–14.

Knop, M., Siegers, K., Pereira, G., Zachariae, W., Winsor, B., Nasmyth, K., and Schiebel, E. (1999). Epitope tagging of yeast genes using a PCR-based strategy: More tags and improved practical routines. Yeast *15*, 963–972.

Kobayashi, T. (2011). Regulation of ribosomal RNA gene copy number and its role in modulating genome integrity and evolutionary adaptability in yeast. Cell. Mol. Life Sci. *68*, 1395–1403.

Kobayashi, T., Horiuchi, T., Tongaonkar, P., Vu, L., and Nomura, M. (2004). SIR2 regulates recombination between different rDNA repeats, but not recombination within individual rRNA genes in yeast. Cell *117*, 441–453.

Køhler, J.B., Jørgensen, M.L.M., Beinoraité, G., Thorsen, M., and Thon, G. (2013). Concerted action of the ubiquitin-fusion degradation protein 1 (Ufd1) and sumo-targeted ubiquitin ligases (STUbLs) in the DNA-damage response. PLoS One *8*, 1–15.

Korsholm, L.M., Gál, Z., Lin, L., Quevedo, O., Ahmad, D.A., Dulina, E., Luo, Y., Bartek, J., and Larsen, D.H. (2019). Double-strand breaks in ribosomal RNA genes activate a distinct signaling and chromatin response to facilitate nucleolar restructuring and repair. Nucleic Acids Res. *47*, 8019–8035.

Lanz, M.C., Dibitetto, D., and Smolka, M.B. (2019). DNA damage kinase signaling: checkpoint and repair at 30 years . EMBO J. *38*.

Liang, J., Singh, N., Carlson, C.R., Albuquerque, C.P., Corbett, K.D., and Zhou, H. (2017). Recruitment of a SUMO isopeptidase to rDNA stabilizes silencing complexes by opposing SUMO targeted ubiquitin ligase activity. Genes Dev. *31*, 802–815.

Lindström, M.S., Jurada, D., Bursac, S., Orsolic, I., Bartek, J., and Volarevic, S. (2018). Nucleolus as an emerging hub in maintenance of genome stability and cancer pathogenesis. Oncogene *37*, 2351–2366.

Mekhail, K., Seebacher, J., Gygi, S.P., and Moazed, D. (2008). Role for perinuclear chromosome

tethering in maintenance of genome stability. Nature *456*, 667–670.

Mérai, Z., Chumak, N., García-Aguilar, M., Hsieh, T.F., Nishimura, T., Schoft, V.K., Bindics, J., Ťusarz, L., Arnoux, S., Opravil, S., et al. (2014). The AAA-ATPase molecular chaperone Cdc48/p97 disassembles sumoylated centromeres, decondenses heterochromatin, and activates ribosomal RNA genes. Proc. Natl. Acad. Sci. U. S. A. *111*, 16166–16171.

Monnat, R.J., Hackmann, A.F.M., and Cantrell, M.A. (1999). Generation of highly site-specific DNA double-strand breaks in human cells by the homing endonucleases I-PpoI and I-CreI. Biochem. Biophys. Res. Commun. *255*, 88–93.

Mooser, C., Symeonidou, I.E., Leimbacher, P.A., Ribeiro, A., Shorrocks, A.M.K., Jungmichel, S., Larsen, S.C., Knechtle, K., Jasrotia, A., Zurbriggen, D., et al. (2020). Treacle controls the nucleolar response to rDNA breaks via TOPBP1 recruitment and ATR activation. Nat. Commun. *11*, 1–16.

Morawska, M., and Ulrich, H.D. (2013). An expanded tool kit for the auxin-inducible degron system in budding yeast. Yeast *30*, 341–351.

Muscarella, D.E., and Vogt, V.M. (1993). A mobile group I intron from Physarum polycephalum can insert itself and induce point mutations in the nuclear ribosomal DNA of saccharomyces cerevisiae. Mol. Cell. Biol. *13*, 1023–1033.

Newman, H.A., Meluh, P.B., Lu, J., Vidal, J., Carson, C., Lagesse, E., Gray, J.J., Boeke, J.D., and Matunis, M.J. (2017). A high throughput mutagenic analysis of yeast sumo structure and function. PLoS Genet. *13*, 1–30.

Nie, M., Aslanian, A., Prudden, J., Heideker, J., Vashisht, A.A., Wohlschlegel, J.A., Yates, J.R., and Boddy, M.N. (2012). Dual recruitment of Cdc48 (p97)-Ufd1-Npl4 ubiquitin-selective segregase by small ubiquitin-like modifier protein (SUMO) and ubiquitin in SUMO-targeted ubiquitin ligase-mediated genome stability functions. J. Biol. Chem. *287*, 29610–29619.

Pabst, S., Döring, L.M., Petreska, N., and Dohmen, R.J. (2019). Methods to study SUMO dynamics in yeast. Methods Enzymol. *618*, 187–210.

Pfander, B., Moldovan, G.L., Sacher, M., Hoege, C., and Jentsch, S. (2005). SUMO-modified PCNA recruits Srs2 to prevent recombination during S phase. Nature *436*, 428–433.

Pieper, G.H., Sprenger, S., Teis, D., and Oliferenko, S. (2020). ESCRT-III/Vps4 Controls Heterochromatin-Nuclear Envelope Attachments. Dev. Cell *53*, 27-41.e6.

Prudden, J., Pebernard, S., Raffa, G., Slavin, D.A., Perry, J.J.P., Tainer, J.A., McGowan, C.H., and Boddy, M.N. (2007). SUMO-targeted ubiquitin ligases in genome stability. EMBO J. *26*, 4089–4101.

Psakhye, I., and Jentsch, S. (2016). Identification of substrates of protein-group SUMoylation. Methods Mol. Biol. *1475*, 219–231.

Richly, H., Rape, M., Braun, S., Rumpf, S., Hoege, C., and Jentsch, S. (2005). A series of ubiquitin binding factors connects CDC48/p97 to substrate multiubiquitylation and proteasomal targeting. Cell *120*, 73–84.

Ryu, T., Spatola, B., Delabaere, L., Bowlin, K., Hopp, H., Kunitake, R., Karpen, G.H., and Chiolo, I. (2015). Heterochromatic breaks move to the nuclear periphery to continue recombinational repair. Nat. Cell Biol. *17*, 1401–1411.

Schindelin, J., Arganda-Carreras, I., Frise, E., Kaynig, V., Longair, M., Pietzsch, T., Preibisch, S.,

Rueden, C., Saalfeld, S., Schmid, B., et al. (2012). Fiji: An open-source platform for biological-image analysis. Nat. Methods *9*, 676–682.

Sherman, F. (2002). Getting started with yeast. In Methods in Enzymology, pp. 3–41.

Shou, W., Hong, J., Moazed, D., Chen, Z.W.S., Charbonneau, H., and Deshaies, R.J. (1999). Exit from Mitosis Is Triggered by Tem1-Dependent Release of the Protein Phosphatase Cdc14 from Nucleolar RENT Complex. Cell *97*, 233–244.

Sinclair, D.A., and Guarente, L. (1997). Extrachromosomal rDNA circles - A cause of aging in yeast. Cell *91*, 1033–1042.

van Sluis, M., and McStay, B. (2015). A localized nucleolar DNA damage response facilitates recruitment of the homology-directed repair machinery independent of cell cycle stage. Genes Dev. *29*, 1151–1163.

Stults, D.M., Killen, M.W., Williamson, E.P., Hourigan, J.S., Vargas, H.D., Arnold, S.M., Moscow, J.A., and Pierce, A.J. (2009). Human rRNA gene clusters are recombinational hotspots in cancer. Cancer Res. *69*, 9096–9104.

Sun, H., Leverson, J.D., and Hunter, T. (2007). Conserved function of RNF4 family proteins in eukaryotes: Targeting a ubiquitin ligase to SUMOylated proteins. EMBO J. *26*, 4102–4112.

Torres-Rosell, J., Sunjevaric, I., De Piccoli, G., Sacher, M., Eckert-Boulet, N., Reid, R., Jentsch, S., Rothstein, R., Aragón, L., and Lisby, M. (2007). The Smc5-Smc6 complex and SUMO modification of Rad52 regulates recombinational repair at the ribosomal gene locus. Nat. Cell Biol. *9*, 923–931.

Tsang, C.K., and Zheng, X.F.S. (2009). Opposing role of condensin and radiation-sensitive gene RAD52 in ribosomal DNA stability regulation. J. Biol. Chem. *284*, 21908–21919.

Tsouroula, K., Furst, A., Rogier, M., Heyer, V., Maglott-Roth, A., Ferrand, A., Reina-San-Martin, B., and Soutoglou, E. (2016). Temporal and Spatial Uncoupling of DNA Double Strand Break Repair Pathways within Mammalian Heterochromatin. Mol. Cell *63*, 293–305.

Udugama, M., Sanij, E., Voon, H.P.J., Son, J., Hii, L., Henson, J.D., Lyn Chan, F., Chang, F.T.M., Liu, Y., Pearson, R.B., et al. (2018). Ribosomal DNA copy loss and repeat instability in ATRX-mutated cancers. Proc. Natl. Acad. Sci. U. S. A. *115*, 4737–4742.

Visintin, R., Hwang, E.S., and Amon, A. (1999). Cfi1 prevents premature exit from mitosis by anchoring Cdc14 phosphatase in the nucleolus. Nature *398*, 818–823.

Warmerdam, D.O., van den Berg, J., and Medema, R.H. (2016). Breaks in the 45S rDNA Lead to Recombination-Mediated Loss of Repeats. Cell Rep. *14*, 2519–2527.

Wright, A.P.H., Carlstedt-Duke, J., and Gustafsson, J.A. (1990). Ligand-specific transactivation of gene expression by a derivative of the human glucocorticoid receptor expressed in yeast. J. Biol. Chem. *265*, 14763–14769.

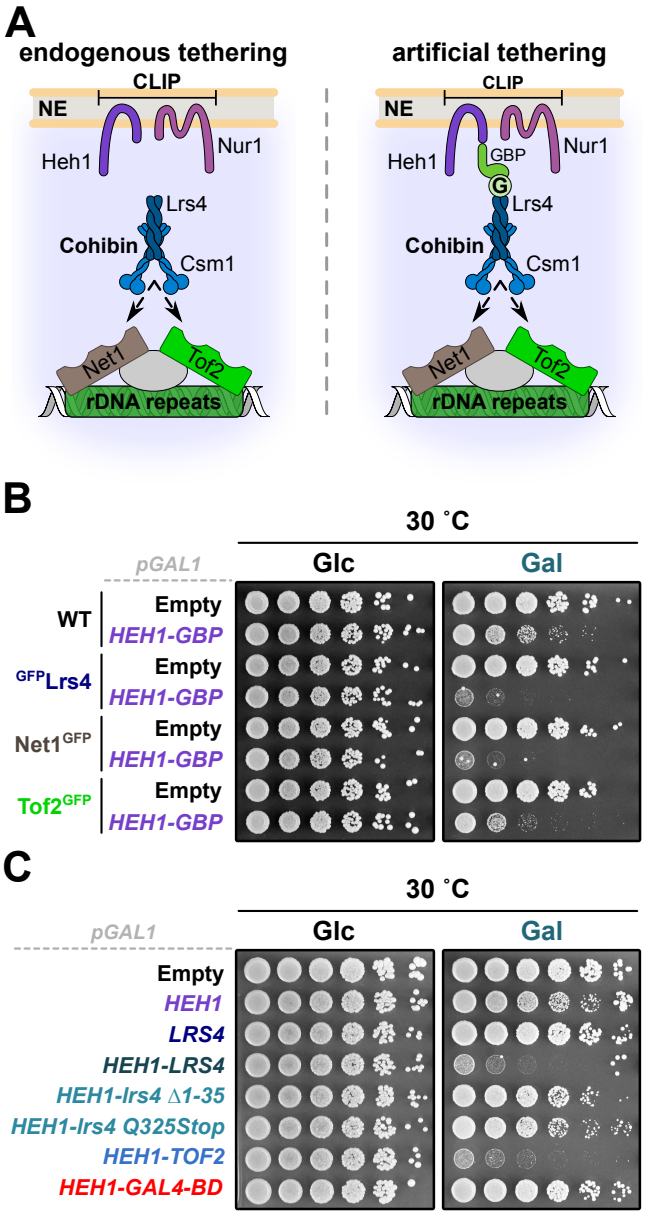

Figure 1. Constitutive perinuclear tethering of rDNA is lethal
(A) Scheme of synthetic rDNA tethering through expression of GFP- and GBP-fusion proteins. Lrs4 binds ribosomal repeats through interaction with the rDNA-bound proteins Net1 or Tof2. G, GFP.
(B) Five-fold serial dilutions of WT, ^{GFP}Lrs4, Net1^{GFP} and Tof2^{GFP} cells transformed with empty vector or a plasmid bearing *HEH1* fused to GFP-binding protein (GBP).
(C) Five-fold serial dilutions of WT cells transformed with empty vector or plasmids bearing the indicated GFP-tagged fusion proteins.
For (B) and (C), cells were spotted and grown on selective media with glucose (control, Glc) or galactose (induction, Gal) at 30˚C for 3 days. All constructs contain the galactose-inducible promoter. See also Figure S1.

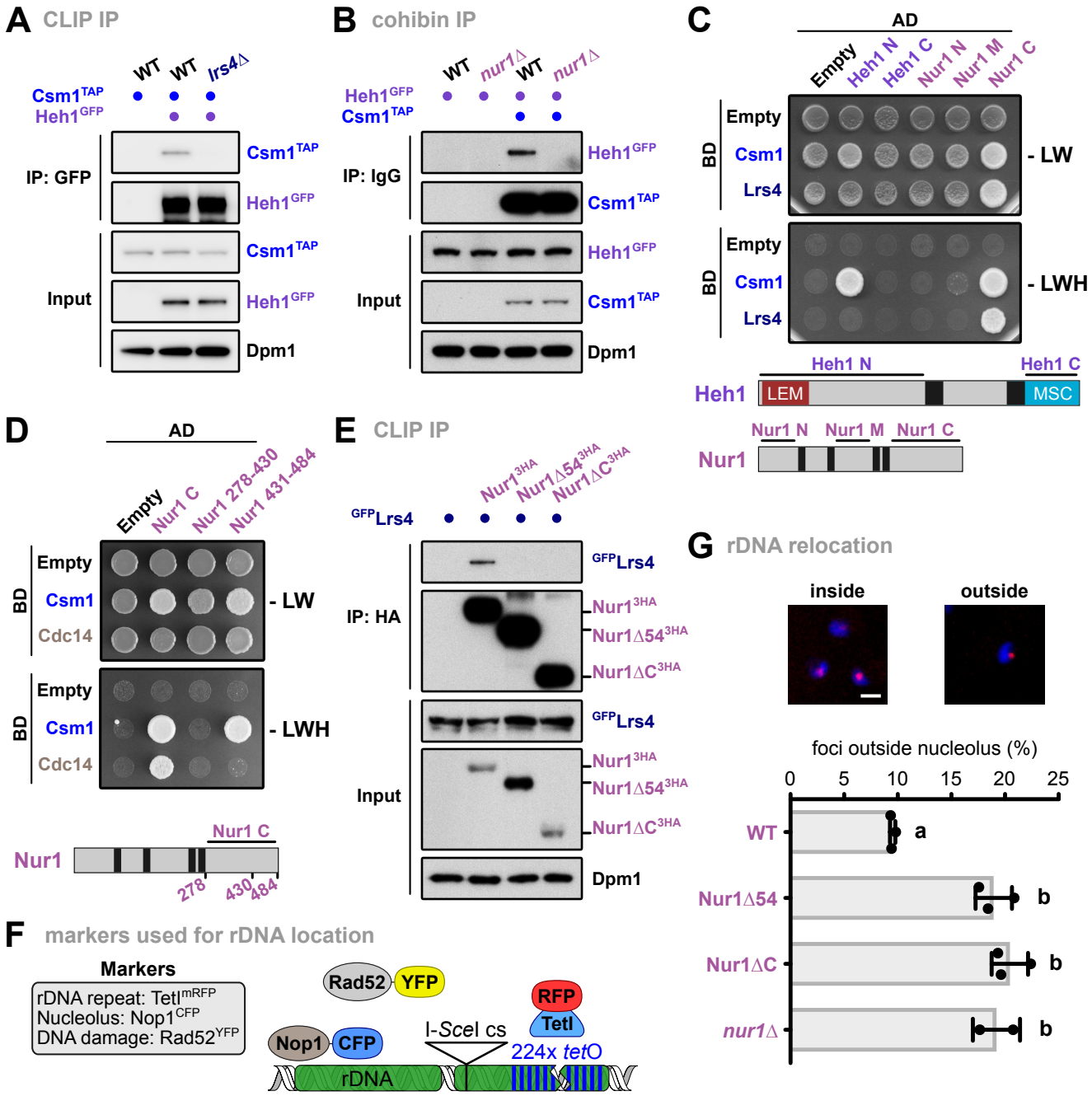

Figure 2. The Nur1 C-terminus is critical for CLIP-cohibin interaction
(A and B) Co-immunoprecipitation of Csm1^{TAP} and Heh1^{GFP} in WT, *lrs4*Δ (A) and *nur1*Δ (B) cells.
(C and D) Y2H analysis of Csm1 and Lrs4 with Heh1 and Nur1 nucleoplasmic domains (C); or of Csm1 and Cdc14 with Nur1 C and truncations (D). Fusions with Gal4-activating domain (AD) or Gal4-DNA-binding domain (BD) are indicated. Cells were spotted on control media (-LW) or selective media (-LWH) and grown for 3 days. Scheme of the constructs used for CLIP complex components is shown.
(E) Co-immunoprecipitation of ^{GFP}Lrs4 with either HA-tagged Nur1 full-length (Nur1^{3HA}), lacking its last 54 residues (Nur1Δ54^{3HA}) or the complete C-terminal domain (Nur1ΔC^{3HA}).
(F) Scheme of rDNA locus and fluorescent markers used in (G). Cells bear a tetO array adjacent to an I-SceI endonuclease cut site inserted into an rDNA unit on chromosome XII, which is revealed by TetImRFP foci. These cells also express Rad52^{YFP} as a marker of the HR machinery. The nucleolus is visualized by a plasmid expressing the nucleolar protein Nop1^{ECFP}.
(G) Percentage of undamaged Nur1^{6HA}, Nur1Δ54^{6HA}, Nur1ΔC^{6HA} or *nur1*Δ cells with rDNA repeats localized outside the nucleolus. Repeat location was monitored by the position of TetImRFP focus relative to the nucleolar mark, and quantification is shown. Data are mean of n = 2-3 independent biological replicates. Representative images are shown. Scale bar, 2 µm. Analysis of variance (ANOVA) was performed, and different letters denote significant differences with a Tukey's *post hoc* test at $P < 0.05$.
For immunoblots, Dpm1 served as loading control. See also Figure S2.

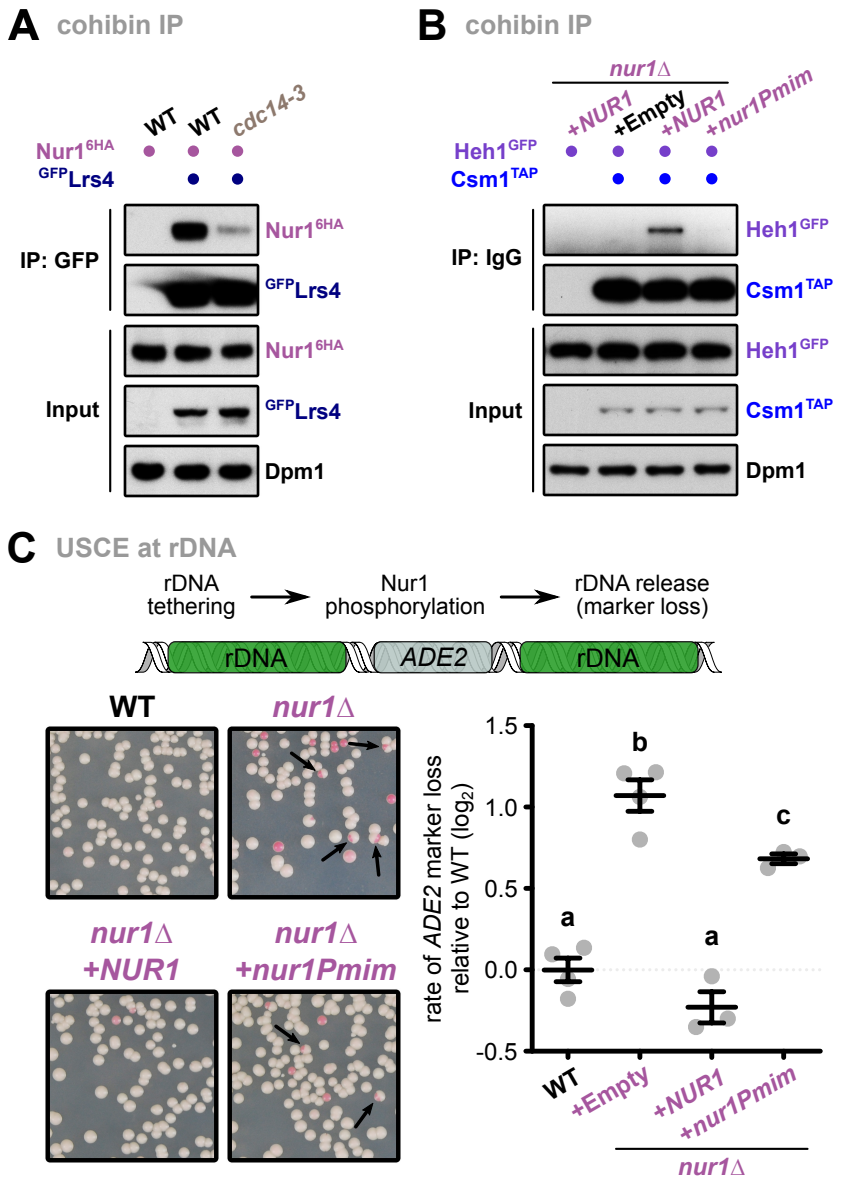

Figure 3. C-terminal Nur1 phosphorylation disrupts the rDNA tethering complex
(A) Co-immunoprecipitation of Nur1^{6HA} with ^{GFP}Lrs4 in WT or *cdc14-3* mutant cells. Cells were grown at the permissive temperature and shifted to 37˚C for 1h.
(B) Co-immunoprecipitation of Heh1^{GFP} with Csm1^{TAP} in *nur1*Δ cells. The strains were transformed with empty vector or plasmids bearing *NUR1* or its phosphomimetic mutant (*nur1Pmim*) expressed from the endogenous promoter.
(C) Quantification of rDNA recombination rates in WT or *nur1*Δ cells as measured by unequal sister chromatid exchange (USCE) using the *ADE2* marker inserted into rDNA. Cells have been transformed with empty vector or plasmids bearing *NUR1* or *nur1Pmim* expressed from the endogenous promoter. The rate of marker loss is calculated as the ratio of half-sectored colonies (as indicated by the arrows) to the total number of colonies, excluding completely red colonies, shown in $\log_2$ scale relative to WT. Data are mean of n = 3-4 independent biological replicates. ANOVA was performed, and different letters denote significant differences with a Tukey's *post hoc* test at $P < 0.05$.
For immunoblots, Dpm1 served as loading control. See also Figure S3.

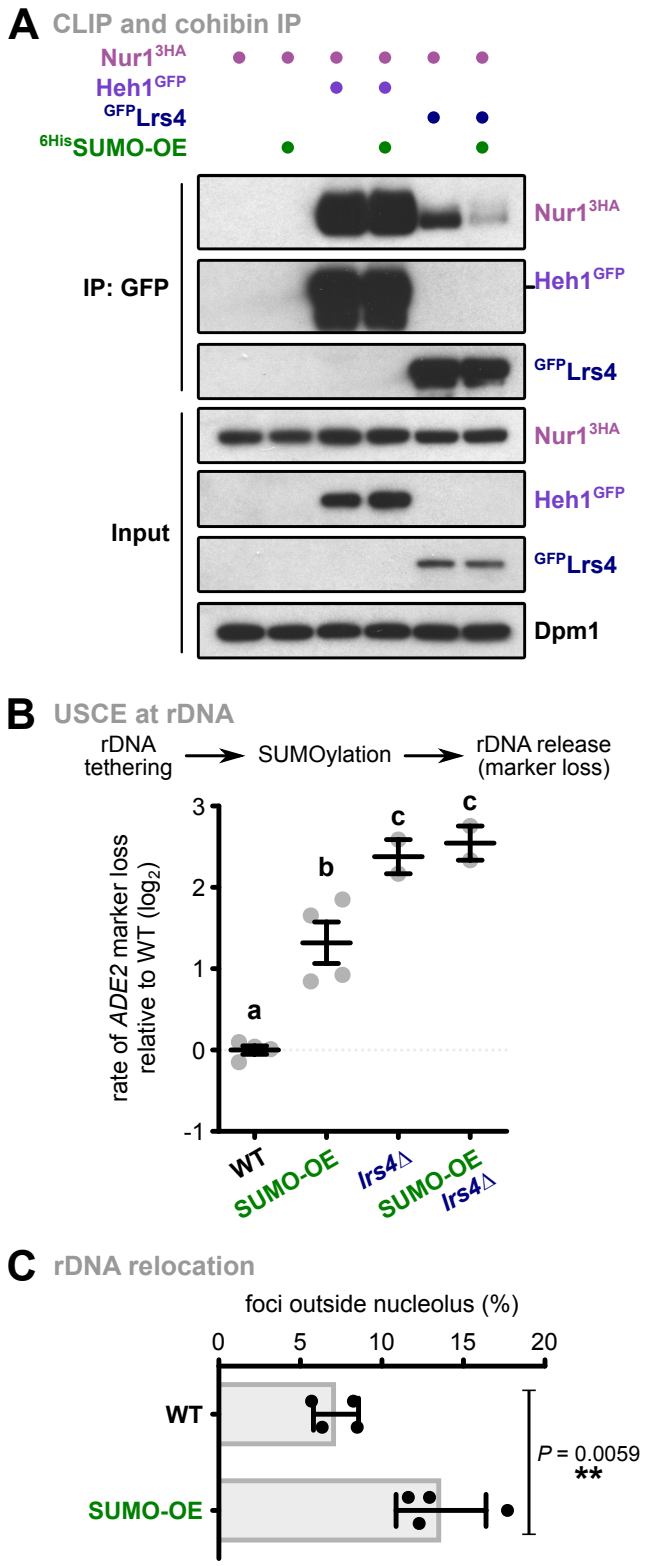

Figure 4. SUMO overexpression promotes CLIP-cohibin disassembly and rDNA relocation and recombination

(A) Co-immunoprecipitation of Nur1^{3HA} with Heh1^{GFP} or ^{GFP}Lrs4 in cells expressing SUMO at endogenous levels or overexpressed from the *ADH1* promoter (^{6His}SUMO-OE). Dpm1 served as loading control.

(B) Rates of unequal rDNA recombination in WT or *lrs4*Δ cells expressing SUMO at endogenous levels or overexpressed from vectors with the *GAL1* promoter (SUMO-OE), grown in galactose-containing media for 4 days. Data are mean of n = 4 independent biological replicates for WT cells, and n = 2 for *lrs4*Δ strains, shown in $\log_2$ scale relative to WT. Marker loss is calculated as in Figure 3.

(C) Percentage of undamaged cells with endogenous (WT) or overexpressed (SUMO-OE) SUMO levels with rDNA repeats localized outside the nucleolus, monitored as described for Figure 2. Quantification of the marked rDNA unit was scored from 4 independent biological replicates, and the mean is shown.

Analysis of variance was performed, and different letters denote significant differences with a Tukey's *post hoc* test at $P < 0.05$. See also Figure S4.

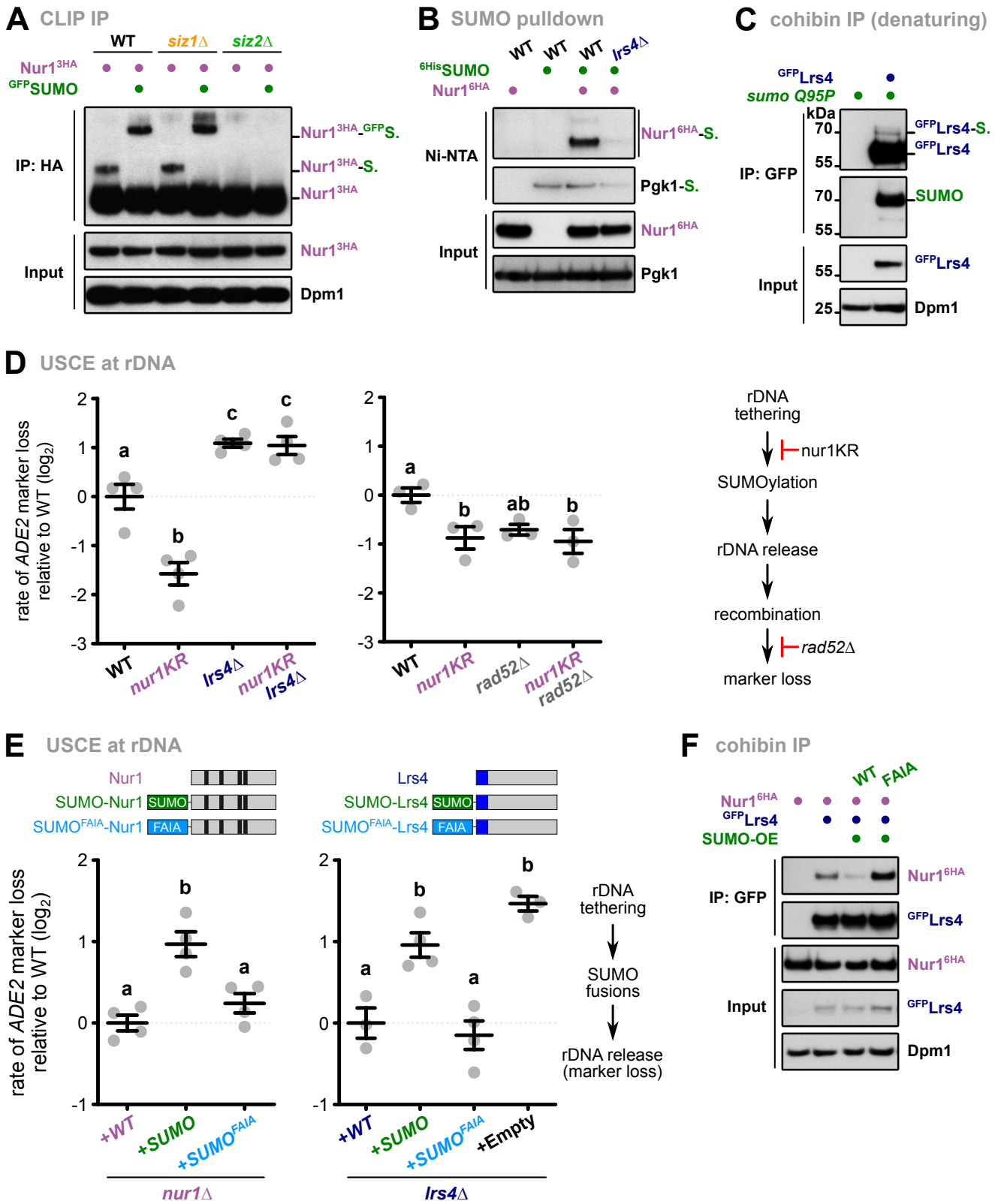

Figure 5. SUMOylation of Nur1 and Lrs4 triggers CLIP-cohibin dissociation

(A) Immunoprecipitation of Nur1^{3HA} in WT, *siz1*Δ and *siz2*Δ expressing SUMO (endogenous promoter) or ^{GFP}SUMO (*ADH1* promoter). Bands corresponding to Nur1 unmodified or monoSUMOylated are labeled.

(B) Denaturing Ni-NTA pulldowns of ^{6His}SUMO conjugates from WT or *lrs4*Δ cells expressing and Nur1^{6HA}, as indicated. Pgk1 SUMOylation was analyzed to control for pulldown efficiency, while unmodified Pgk1 served as loading control.

(C) Immunoprecipitation under semi-denaturing conditions of ^{GFP}Lrs4 in cells overexpressing a isopeptidase-resistant SUMO mutant (SUMO^{Q95P}). Detection of SUMO from immunoprecipitated samples is shown.

(D) Rates of unequal rDNA marker loss in WT, *lrs4*Δ (left) or *rad52*Δ (right) cells expressing endogenously 6HA-tagged Nur1 or the SUMOylation deficient Nur1 K175-176R mutant (*nur1KR*).

(E) Rates of unequal rDNA marker loss in *nur1*Δ or *lrs4*Δ cells transformed with empty vector or plasmids bearing 3HA-tagged *NUR1* (left), TAP-tagged *LRS4* (right) or the indicated linear fusions with the endogenous promoter, as indicated. Used constructs for Nur1 and Lrs4 are shown. Black lines depict the predicted transmembrane domains of Nur1. Lrs4 is shown in blue (Csm1-interacting region) and light grey (C-terminal uncharacterized region).

(F) Co-immunoprecipitation of Nur1^{6HA} with ^{GFP}Lrs4 in cells with endogenous SUMO levels, or strains overexpressing either SUMO WT or a mutant unable to recognize SIMs (FAIA, which harbors the mutations F37A I39A). The different strains were grown to mid-log phase, and SUMO variants were induced by adding 2% galactose for 2 h 30'.
For (A), (C) and (F), Dpm1 served as loading control. For (D) and (E), the rate of marker loss is calculated as in Figure 3; data are the mean of n = 3-4 independent biological replicates, shown in $\log_2$ scale relative to WT. ANOVA was performed, and different letters denote significant differences with a Tukey's *post hoc* test at $P < 0.05$. See also Figure S5.

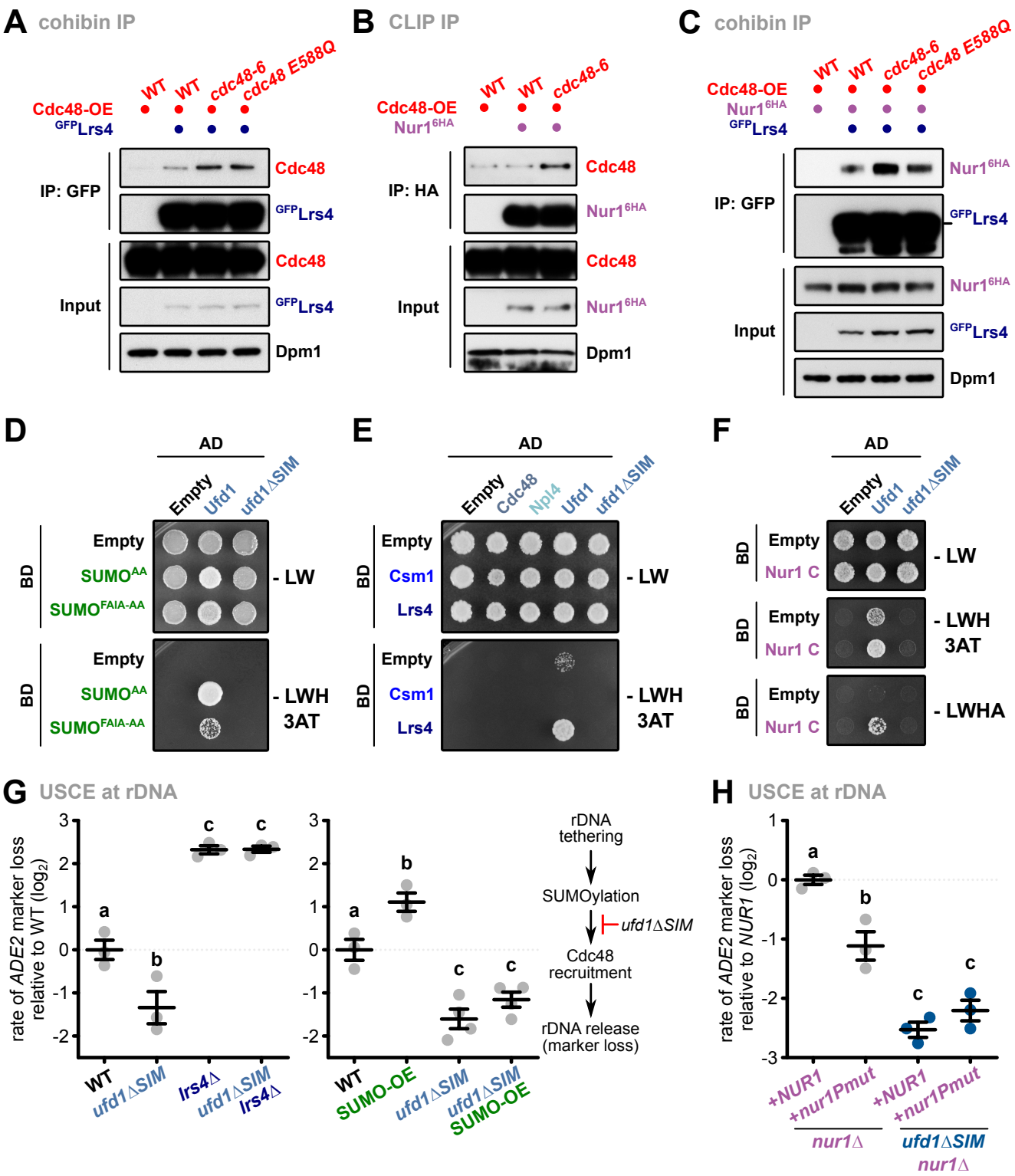

Figure 6. SUMOylation recruits Cdc48 via its co-factor Ufd1 to assist in rDNA release
(A and B) Co-immunoprecipitation of Cdc48 with ^{GFP}Lrs4 (A) or Nur1^{6HA} (B) in cells overexpressing WT or mutant Cdc48.
(C) Co-immunoprecipitation of Nur1^{6HA} with ^{GFP}Lrs4 in cells overexpressing WT or mutant Cdc48.
(D) Y2H analysis of conjugation-deficient SUMO (SUMO^{AA}) or the F37A I39A mutant unable to recognize SIMs (SUMO$^{FAIA-AA}$) (as a Gal4-DNA-binding domain fusion, BD) with Ufd1 and ufd1ΔSIM (as a Gal4-activating domain fusion, AD).
(E) Y2H analysis of Csm1 and Lrs4 with Cdc48, Npl4, Ufd1 and ufd1ΔSIM. Fusions with Gal4-activating domain (AD) or Gal4-DNA-binding domain (BD) are indicated.
(F) Y2H analysis of Nur1 C (BD) with Ufd1 and ufd1ΔSIM (AD), as indicated.
(G) Rates of unequal rDNA recombination in WT, *ufd1ΔSIM*, *lrs4Δ* or *ufd1ΔSIM lrs4Δ* cells (left), in WT and ufd1ΔSIM strains expressing SUMO at endogenous levels or overexpressed from vectors with the *TEF1* promoter (SUMO-OE) (right).

(H) Rates of unequal rDNA recombination in *nur1*Δ and *nur1*Δ *ufd1*Δ*SIM* cells transformed with plasmids bearing *NUR1* or its phosphomutant version (*nur1Pmut*) with the *GAL1* promoter. Cells were grown in galactose-containing media for 4 days.

For (A) and (C), the different strains were grown to mid-log phase, and Cdc48 variants were induced by adding 2% galactose for 2 h 30'; Dpm1 served as loading control. For (D), (E) and (F), cells were spotted on control media (-LW) or selective media (-LWH + 3AT 1 mM) and grown for 3 days, or spotted on -LWHA selective media and grown for 4 days (F). For (G) and (H), the rate of marker loss is calculated as in Figure 3; data are mean of n = 3-4 independent biological replicates, shown in $\log_2$ scale relative to WT (G) or *nur1*Δ+*NUR1* (H). ANOVA test was used, and different letters denote significant differences with a Tukey's *post hoc* test at $P < 0.05$.

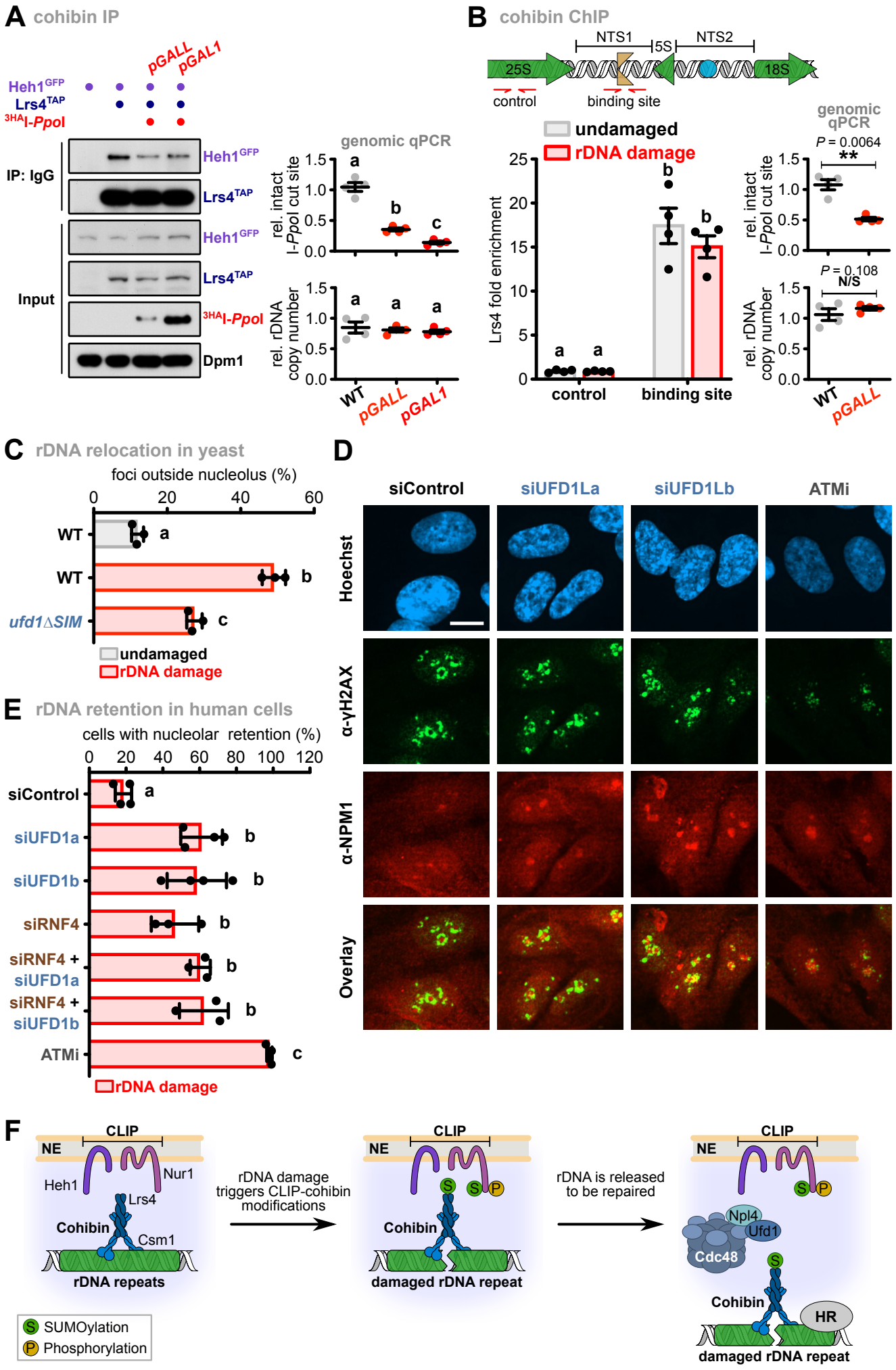
A cohibin IP
pGALL
pGAL1
Heh1GFP
Lrs4TAP
3HAI-PpoI
IP: IgG
Input
Dpm1
genomic qPCR
rel. intact I-PpoI cut site
rel. rDNA copy number
WT
pGALL
pGAL1
B cohibin ChIP
NTS1
5S
NTS2
25S
18S
control
binding site
undamaged
rDNA damage
Lrs4 fold enrichment
genomic qPCR
P = 0.0064
**
P = 0.108
N/S
C rDNA relocation in yeast
foci outside nucleolus (%)
ufd1ΔSIM
undamaged
rDNA damage
D
siControl
siUFD1La
siUFD1Lb
ATMi
Hoechst
α-γH2AX
α-NPM1
Overlay
E rDNA retention in human cells
cells with nucleolar retention (%)
siUFD1a
siUFD1b
siRNF4
siRNF4 + siUFD1a
siRNF4 + siUFD1b
rDNA damage
F
CLIP
NE
Heh1
Nur1
Lrs4
Cohibin
Csm1
rDNA repeats
rDNA damage triggers CLIP-cohibin modifications
damaged rDNA repeat
rDNA is released to be repaired
Npl4
Ufd1
Cdc48
HR
SUMOylation
Phosphorylation

Figure 7. DNA damage contributes to CLIP-cohibin disassembly and Cdc48/p97-dependent rDNA relocation
(A) Co-immunoprecipitation of Heh1^{GFP} with Lrs4^{TAP} in cells with or without rDNA damage. Dpm1 served as loading control. ^{3HA}I-*Ppo*I with the galactose-inducible promoters *GALL* and *GAL1* were integrated at the *LEU2* locus.
(B) Lrs4^{TAP} binding to rDNA repeats in cells with or without rDNA damage, quantified by ChIP-qPCR. The ChIP values are shown as Lrs4 fold enrichment over the average of three rDNA positions, after normalization to input. Illustration shows a schematic representation of an rDNA unit. Amplified regions are highlighted with red arrows.
(C) Percentage of WT and *ufd1*Δ*SIM* cells with rDNA repeats localized outside the nucleolus before and after DSB induction. Relative nucleolar location of rDNA repeats was monitored and quantified as described for Figure 2.
(D) Retention of rDNA locus (NPM1) in human cells upon DNA damage treated with siRNA against UFD1L. Human RPE cells stably expressing FKBP12-^{HA}I-*Ppo*I were transfected with siRNAs against UFD1L (siUFD1La and siUFD1Lb), or treated with the ATM kinase inhibitor KU55933 (ATMi). DSBs were induced by incubation of the cell lines in the presence of doxycycline for 4 h and shield-1 for 1 h. Representative images of immunofluorescence staining after rDNA damage, using the indicated antibodies, are shown. Scale bar, 5 μm.
(E) Quantification of human RPE cells transfected with siRNA against RNF4 (siRNF4), siUFD1L (siUFD1La and siUFD1Lb), or combination thereof, showing the percentage of cells with nucleolar retention of γH2AX foci, defined as cells that show an overlap (yellow) of the γH2AX (green) with the NPM (red) signal.
(F) Model: under normal conditions, the rDNA repeats are kept inside the nucleolus by Cdc14-mediated dephosphorylation of Nur1, which maintains the interaction of the rDNA tethering complex. When a repeat unit is damaged, SUMOylation of CLIP-cohibin disrupts the complex through Cdc48-Npl4-Ufd1, allowing rDNA relocation outside the nucleolus. Nur1 is also phosphorylated, further supporting the broken repeat relocation.
For (A), (B) and (C), the strains were grown to mid-log phase, and the endonuclease was induced by adding 2% galactose for 2 h (A and C) or 1.5 h (B). For (A) and (B), quantification of double-strand break (DSB) induction (top right) and rDNA copy number (bottom right) relative to undamaged cells is shown. For (B), (C) and (E), data are mean of n = 3-4 biologically independent experiments. ANOVA was performed, and different letters denote significant differences with a Tukey's *post hoc* test at $P < 0.05$. N/S, not significant. See also Figure S7.

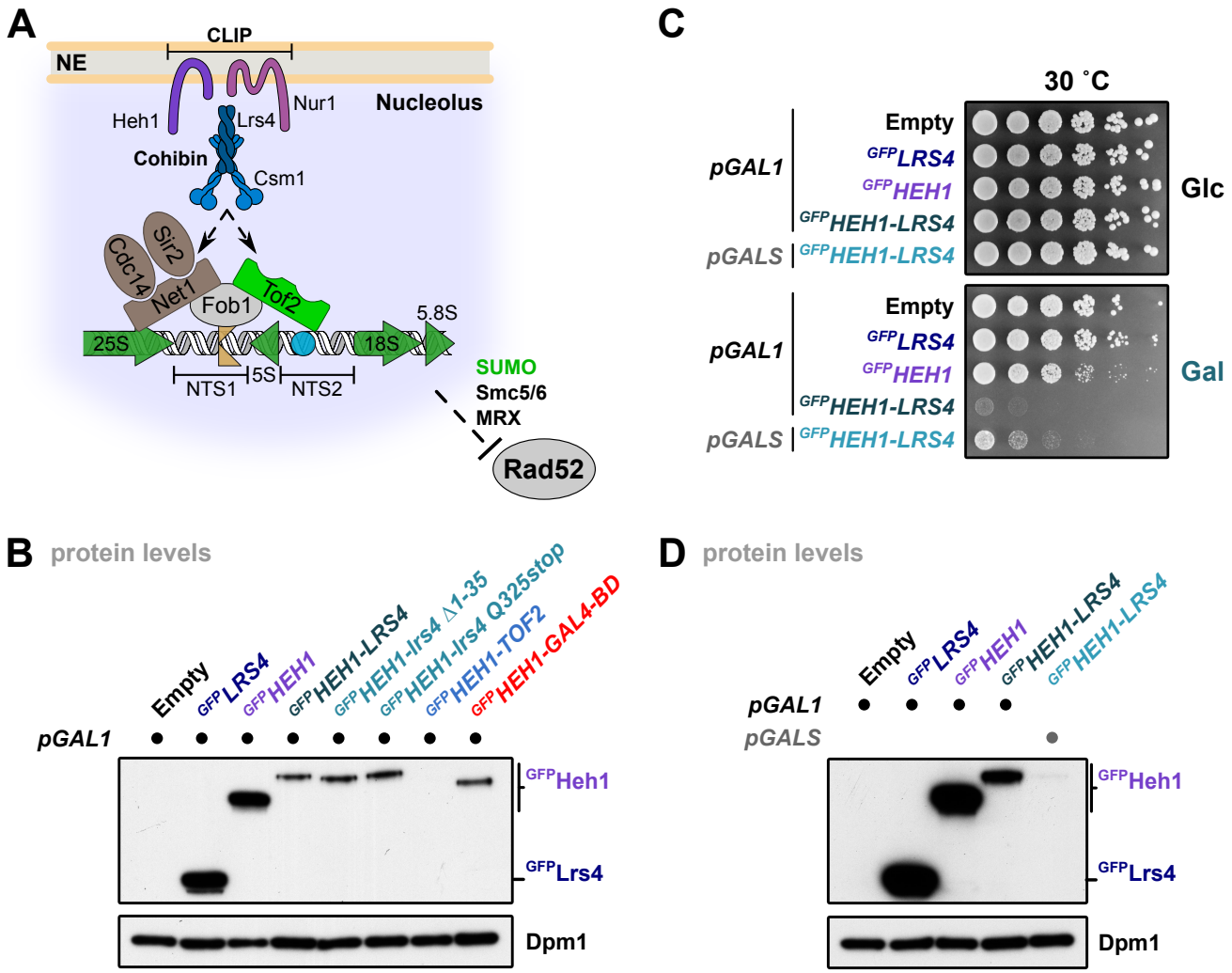

Figure S1. Disruption of rDNA dynamics causes severe growth defects in yeast. Related to Figure 1
(A) Scheme of an rDNA unit bound by the tethering complex in *Saccharomyces cerevisiae*. Each repeat of 9.1 kb presents a near-identical sequence comprising the 35S (subdivided in 5.8S, 18S and 25S) and 5S ribosomal RNA coding genes. Polymerase II silenced regions are known as NTS1 (non-transcribed spacer 1) and NTS2 regions, which are located down- and upstream of the 5S gene, respectively. NTS1 contains the replication fork barrier (RFB), whereas NTS2 contains an autonomous replicating sequence (ARS). The rDNA units are attached to the inner nuclear membrane via interaction between cohibin (Lrs4 and Csm1) and CLIP (Heh1 and Nur1). Cohibin then binds to the NTS1 region of the rDNA repeats through an rDNA-bound protein complex that includes Fob1, Tof2 and the RENT complex (regulator of nucleolar silencing and telophase exit; composed of Cdc14, Net1 and Sir2). SUMO together with the MRX and Smc5/6 complexes exclude Rad52 from the nucleolus.
(B) Immunoblot of WT cells transformed with empty vector or plasmids bearing GFP-tagged *LRS4*, *HEH1* or fusion proteins with the galactose-inducible promoter after induction.
(C) Five-fold serial dilutions of WT cells transformed with empty vector or plasmids bearing the indicated GFP-tagged fusion proteins with different galactose-inducible promoters (either *pGAL1* or *pGALS*), as indicated. Cells were spotted and grown on selective media with glucose (control, Glc) or galactose (induction, Gal) at 30˚C for 3 days.
(D) Immunoblot of the strains used in (C), after galactose induction.
For (B) and (D), the different strains were grown to mid-log phase, fusion proteins were induced by adding 2% galactose for 2 h 30'. Dpm1 served as loading control.

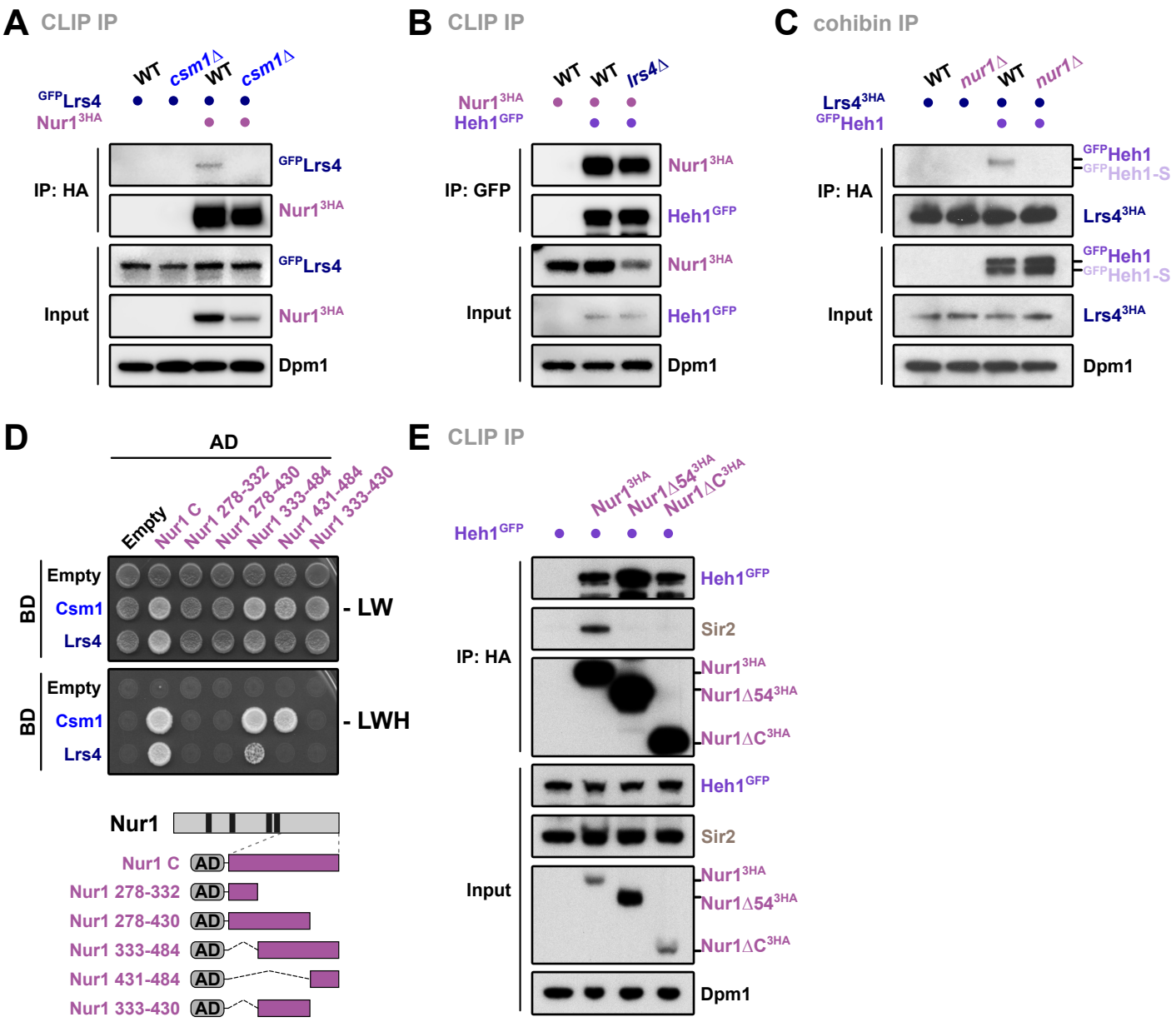

Figure S2. The C-terminal residues of Nur1 are required for CLIP-cohibin complex formation. Related to Figure 2

(A to C) Co-immunoprecipitation of ^{GFP}Lrs4 with Nur1^{3HA} in WT or *csm1*Δ cells (A); of Nur1^{3HA} with Heh1^{GFP} in WT or *lrs4*Δ cells (B); and of ^{GFP}Heh1 with Lrs4^{3HA} in WT and *nur1*Δ cells (C). Due to N-terminal tagging of Heh1, both spliced versions (denoted as Heh1 and Heh1-S) can be detected in (C).

(D) Y2H analysis of Csm1 and Lrs4 with either Nur1 C or truncated mutants. Fusions with Gal4-activating domain (AD) or Gal4-DNA-binding domain (BD) are indicated. Schematic showing Nur1 truncated constructs.

(E) Co-immunoprecipitation of Heh1^{GFP} and Sir2 with either HA-tagged Nur1 full-length (Nur1^{3HA}), lacking its last 54 residues (Nur1Δ54^{3HA}) or the complete C-terminal domain (Nur1ΔC^{3HA}).

For immunoblots, Dpm1 served as loading control. For Y2H assays, cells were spotted on control media (-LW) or selective media (-LWH) and grown for 3 days.

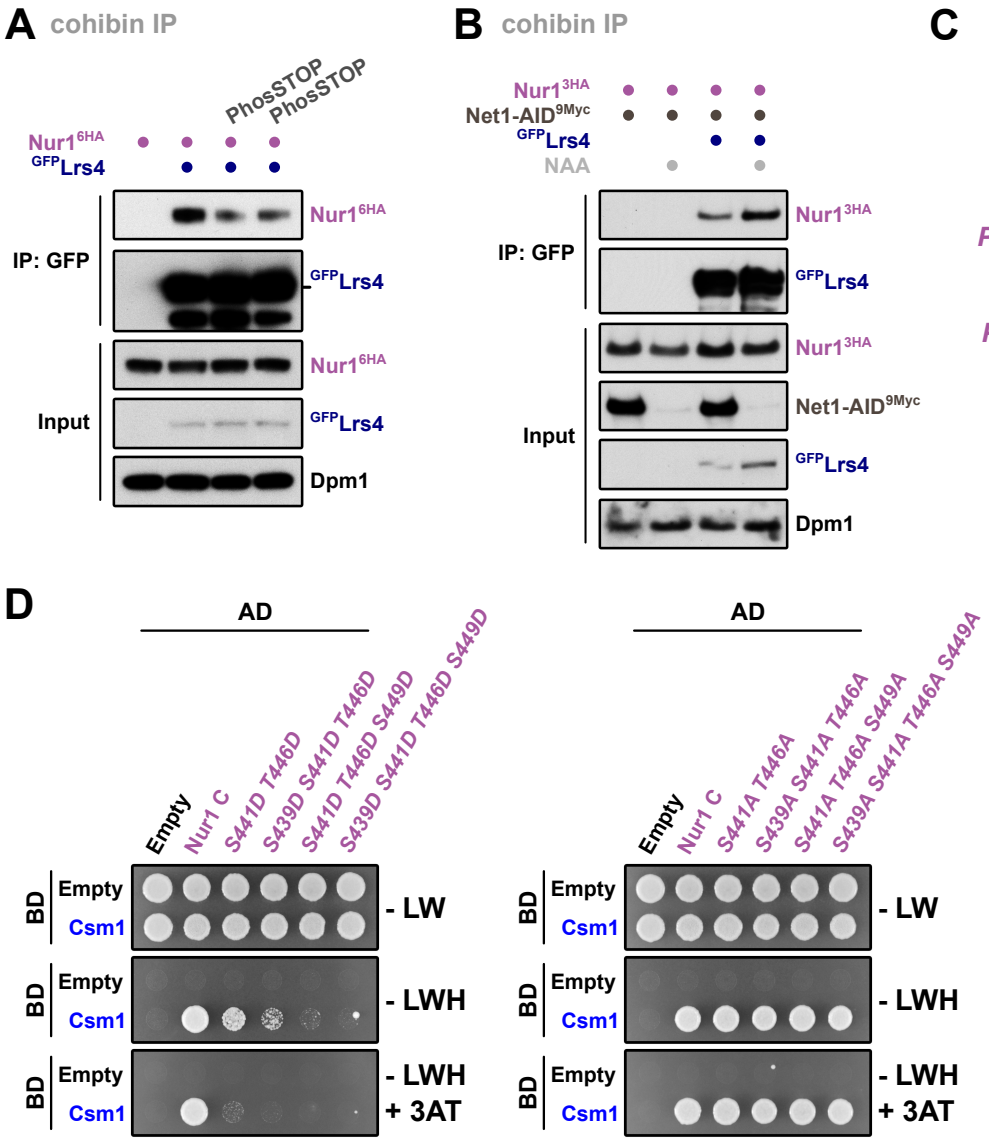

Figure S3. Phosphorylation of C-terminal Nur1 impairs CLIP-cohibin interaction. Related to Figure 3
(A) Co-immunoprecipitation of Nur1^{3HA} with ^{GFP}Lrs4 in WT with impaired global phosphatase activity (PhosSTOP). One untreated and two independently treated samples are shown.
(B) Co-immunoprecipitation of Nur1^{3HA} with ^{GFP}Lrs4 in WT or Net1-depleted cells. Degradation of a C-terminal AID (auxin inducible degron) fusion of Net1 (Net1-AID^{9Myc}) was induced through treatment with 1-naphthaleneacetic acid 1.5 mM (NAA, a synthetic analog of auxin) for 2 h.
(C) Schematic highlighting Nur1 residues important for CLIP-cohibin interaction in red. Amino acids 439 to 449 are depicted. P, phosphorylation.
(D) Y2H analysis of Csm1 (BD) with Nur1 C and phosphomimetic (left) or phosphomutant (right) constructs (AD), as indicated.
For immunoblots, Dpm1 served as loading control. For Y2H assays, cells were spotted on control media (-LW) or selective media (-LWH or -LWH + 3AT 1 mM) and grown for 3 days.

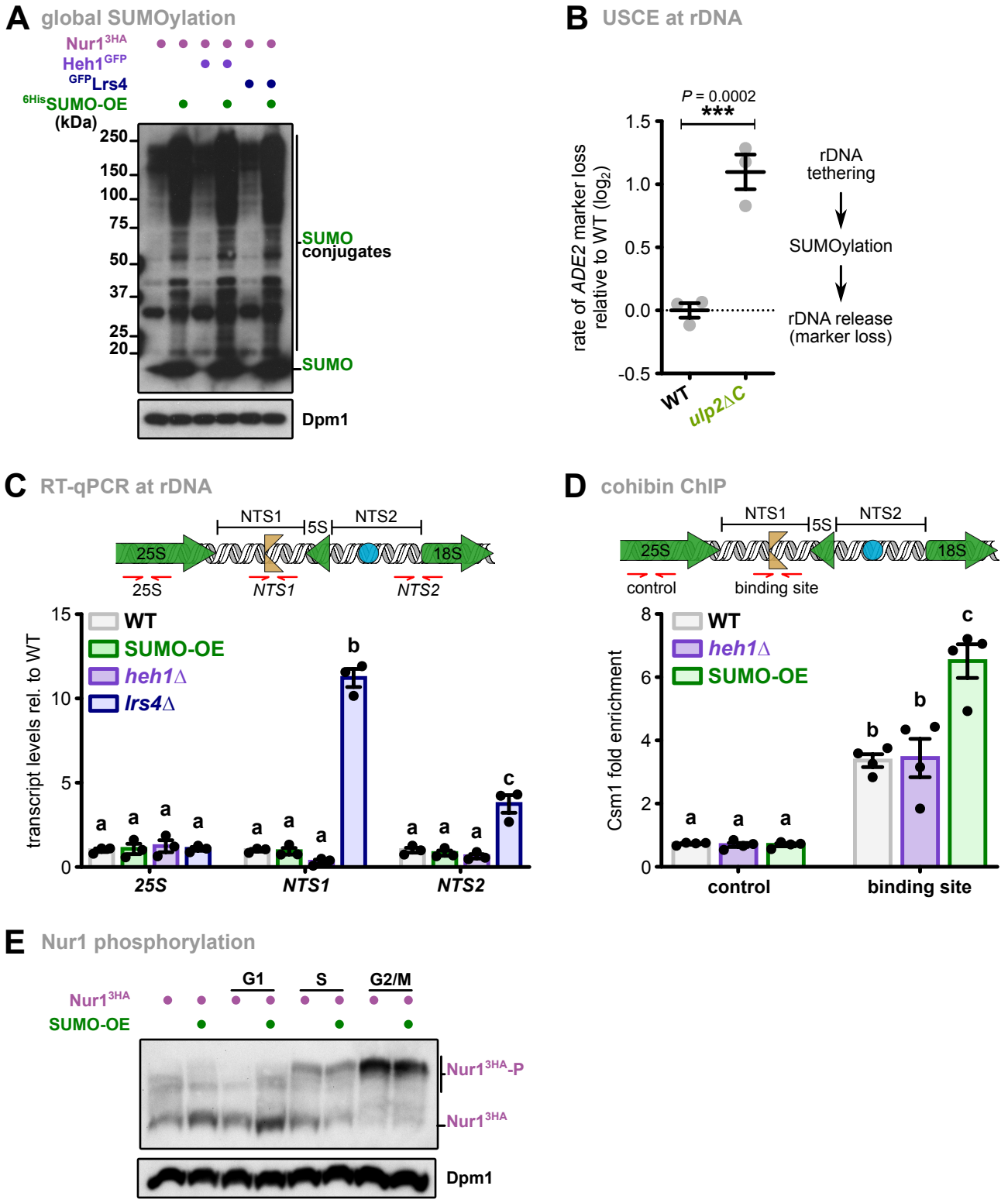

Figure S4. Overexpression of SUMO increases rDNA instability by releasing the repeats from the nucleolus. Related to Figure 4

(A) Immunoblot of SUMO conjugates of cells from Figure 4A, expressing SUMO at endogenous levels or overexpressed from the *ADH1* promoter (^{6His}SUMO-OE).

(B) Rates of unequal rDNA recombination in WT and *ulp2ΔC* cells. The rate of marker loss is calculated as the ratio of half-sectored colonies to the total number of colonies, excluding completely red colonies; data is shown in log_2 scale relative to WT.

(C) RT-qPCR analysis of WT, SUMO-OE, *heh1Δ* and *lrs4Δ* strains. Shown are transcript levels relative to WT after normalization to *ACT1*. Illustration shows a schematic representation of an rDNA unit. Amplified regions are highlighted with red arrows. NTS, non-transcribed spacer; yellow symbol, replication fork block; blue symbol, ARS.

(D) Csm1TAP binding to rDNA repeats in WT, *heh1Δ* and SUMO overexpressing (SUMO-OE) cells, quantified by ChIP-qPCR. The ChIP values are shown as Csm1^{TAP} fold enrichment over the average of three rDNA positions, after normalization to input. Scheme of an rDNA repeat as in (C) is shown; in red are marked the amplified regions.

(E) Nur1^{3HA} phosphorylation-dependent mobility shifts in cells expressing SUMO at endogenous levels or overexpressed from the *ADH1* promoter (^{6His}SUMO-OE), analyzed using Phos-tag gels. Cells were arrested in G1, S and G2/M by treating the cells with α-factor, HU 100 mM or nocodazole 5 ug/ml for 2h, respectively.
For immunoblots, Dpm1 served as loading control. For (B), (C) and (D), data are mean of n = 3-4 independent biological replicates. Analysis of variance (ANOVA) was performed, and different letters denote significant differences with a Tukey's *post hoc* test at $P < 0.05$.

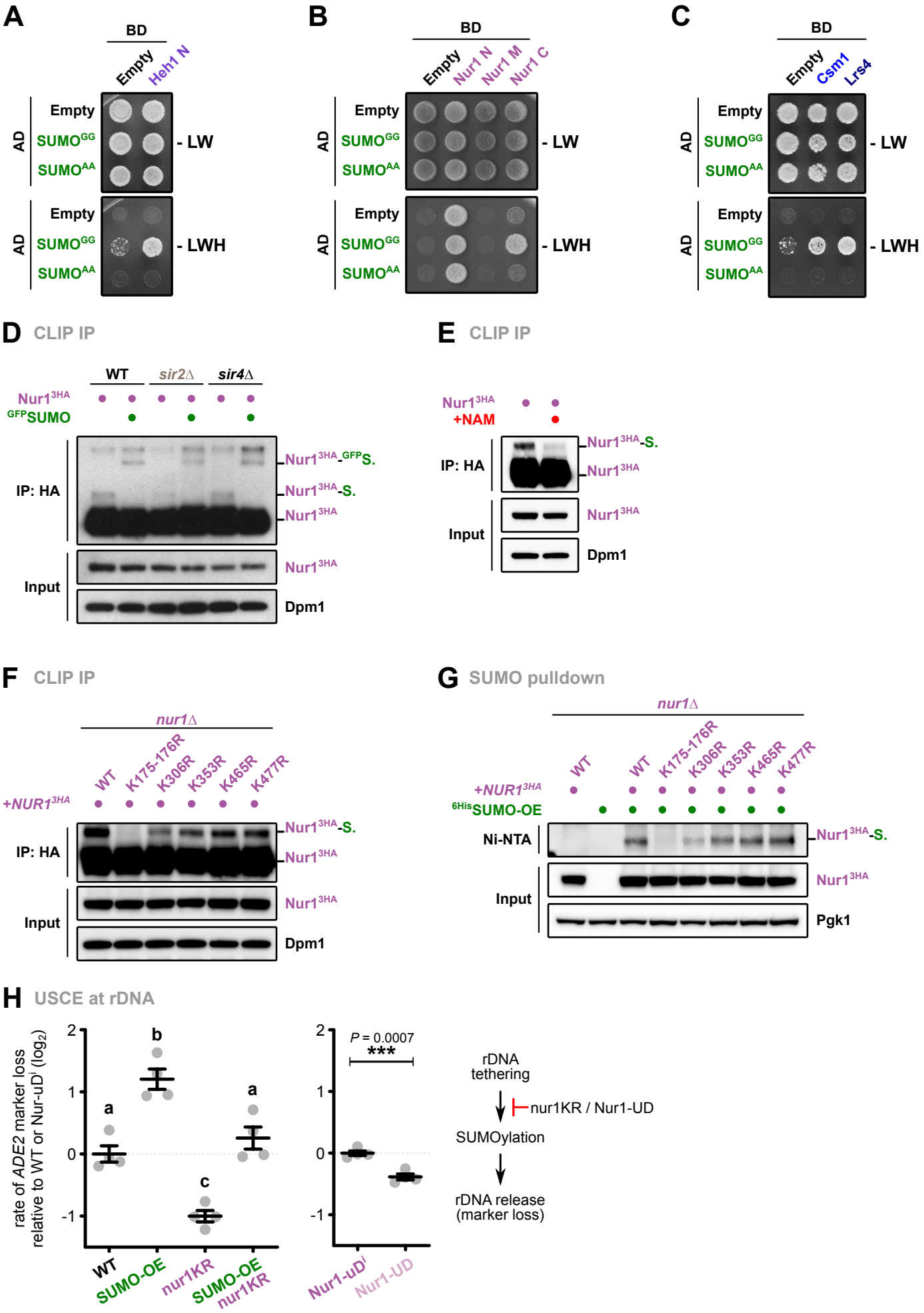
A
BD
Empty
Heh1 N
AD
Empty
SUMO^GG
SUMO^AA
- LW
- LWH
B
Nur1 N
Nur1 M
Nur1 C
C
Csm1
Lrs4
D CLIP IP
WT
sir2Δ
sir4Δ
Nur1^3HA
^GFP^SUMO
IP: HA
Input
Nur1^3HA-^GFP^S.
Nur1^3HA-S.
Dpm1
E CLIP IP
+NAM
F CLIP IP
nur1Δ
+NUR1^3HA
K175-176R
K306R
K353R
K465R
K477R
G SUMO pulldown
^6His^SUMO-OE
Ni-NTA
Pgk1
H USCE at rDNA
rate of ADE2 marker loss relative to WT or Nur-uD^i (log2)
P = 0.0007
***
SUMO-OE
nur1KR
Nur1-uD^i
Nur1-UD
rDNA tethering
nur1KR / Nur1-UD
SUMOylation
rDNA release (marker loss)

Figure S5. SUMOylation of CLIP-cohibin members affects rDNA stability. Related to Figure 5

(A to C) Y2H analysis of ($SUMO^{GG}$) or a conjugation-deficient SUMO ($SUMO^{AA}$) with Heh1 N (A) and Nur1 nucleoplasmic domains (B) or Csm1 and Lrs4 (C). Fusions with Gal4-activating domain (AD) or Gal4-DNA-binding domain (BD) are indicated. Cells were spotted on control media (-LW) or selective media (-LWH) and grown for 3 days.

(D) Immunoprecipitation of $Nur1^{3HA}$ in WT, *sir2*Δ and *sir4*Δ expressing SUMO (endogenous promoter) or ^{GFP}SUMO (*ADH1* promoter). Bands corresponding to Nur1 unmodified or monoSUMOylated are labeled.

(E) Immunoprecipitation of $Nur1^{3HA}$ in WT cells treated with nicotinamide (NAM) 5 mM for 2h. Bands corresponding to Nur1 unmodified or monoSUMOylated are labeled.

(F) Immunoprecipitation of $Nur1^{3HA}$ in *nur1*Δ cells transformed with plasmids bearing *NUR1* or the indicated mutants with the endogenous *NUR1* promoter. Bands corresponding to Nur1 unmodified or monoSUMOylated are labeled.

(G) Denaturing Ni-NTA pulldowns of ^{6His}SUMO conjugates from *nur1*Δ cells transformed with plasmids bearing *NUR1* or the indicated mutants with the endogenous *NUR1* promoter. Pgk1 served as loading control.

(H) Rates of unequal rDNA recombination in WT cells expressing Nur1 or the SUMOylation deficient mutant nur1KR with endogenous or increased levels of SUMO, grown in galactose-containing media (left); and of strains expressing Nur1 fused to the SUMO-protease domain of Ulp1 (Nur1-UD) or the inactive version (Nur1-uD^i), which carries the F474A and C580S mutations (right). For SUMO overexpression, the different strains were transformed with empty vector or a plasmid bearing SUMO with the *GAL1* promoter. The rate of marker loss is calculated as the ratio of half-sectored colonies to the total number of colonies, excluding completely red colonies, shown in log_2 scale relative to WT (left) or Nur1-uD^i (right); data are mean of n = 4 independent biological replicates. Analysis of variance (ANOVA) was performed, and different letters denote significant differences with a Tukey's *post hoc* test at $P < 0.05$.

For (D), (E) and (F), Dpm1 served as loading control.

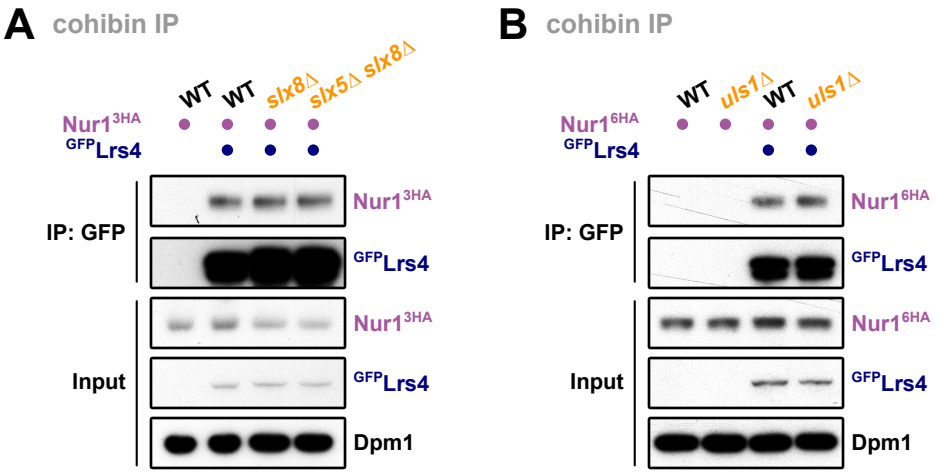

Figure S6. CLIP-cohibin interaction is not affected by the STUbLs
(A and B) Co-immunoprecipitation of HA-tagged Nur1 with ^{GFP}Lrs4 in WT, *slx8*Δ, *slx5*Δ *slx8*Δ (A), or *uls1*Δ (B) cells, as indicated. Dpm1 served as loading control.

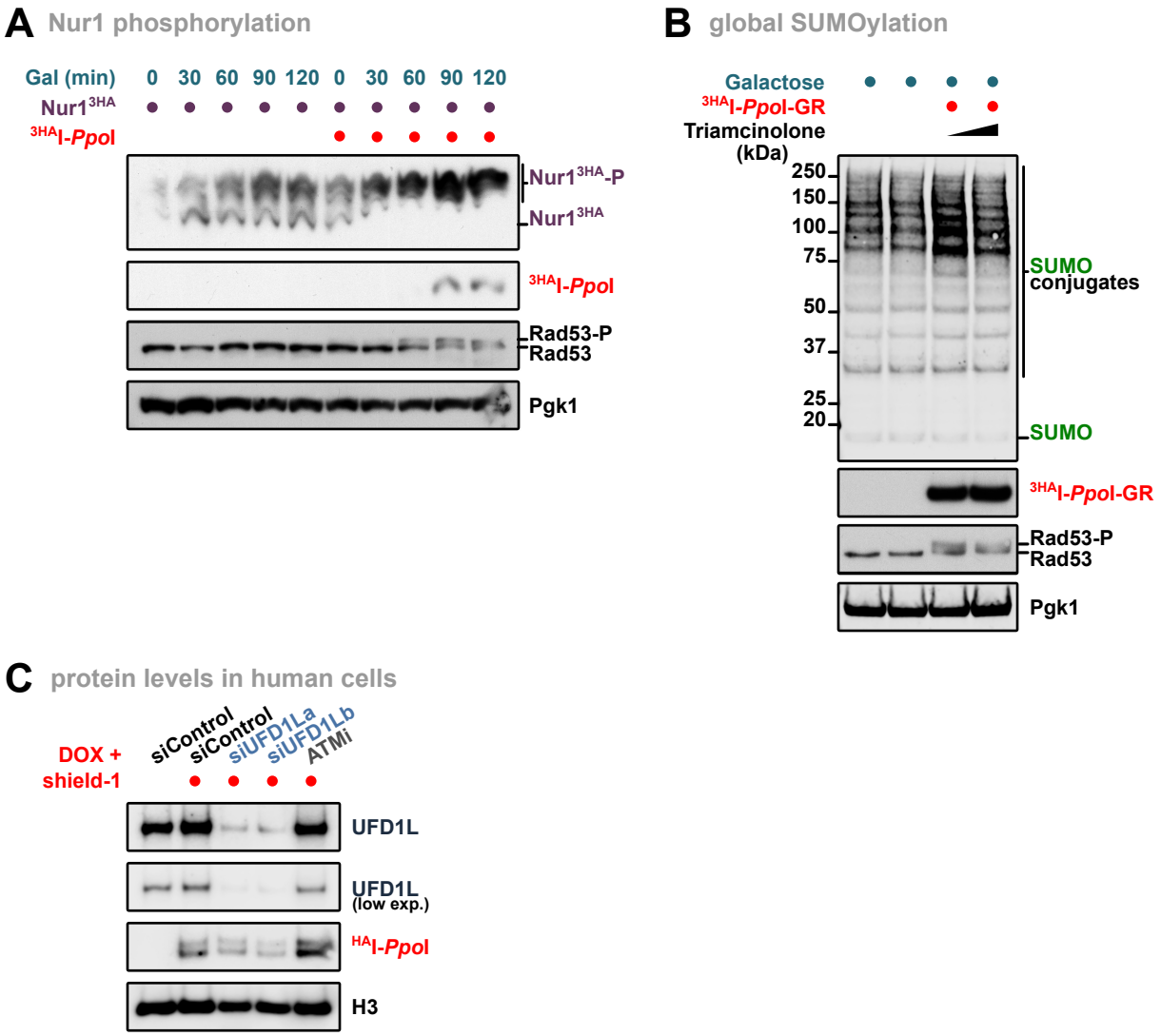

Figure S7. Damage at rDNA promotes release of broken repeats. Related to Figure 7
(A) Nur1^{3HA} phosphorylation-dependent mobility shifts cells in cells with or without rDNA damage, analyzed using Phos-tag gels. Dpm1 served as loading control. ^{3HA}I-*Ppo*I with the galactose-inducible promoters *GALL* were integrated at the *LEU2* locus. The different strains were grown to mid-log phase, and the endonuclease was induced by adding 2% galactose for indicated times.
(B) Immunoblot of SUMO conjugates upon rDNA damage. To ensure tight regulation of the endonuclease, I-*Ppo*I was fused to the glucocorticoid receptor ligand-binding domain (^{3HA}I-*Ppo*I-GR) and expressed under the galactose-inducible promoter GAL1 from a centromeric plasmid *YCplac22*. The strains were grown to mid-log phase, and the endonuclease was induced by adding 2% galactose for 3 h. Nuclear location of ^{3HA}I-*Ppo*I-GR was induced by addition of triamcinolone acetonide 7.5 µM and 75 µM.
(C) Immunoblot of RPE cells from Figure 7D after rDNA damage, showing knock-down efficiency of UFD1L and ^{HA}I-*Ppo*I induction. H3 served as loading control.
For (A) and (B), Rad53 phosphorylation served as a marker for DNA damage, while Pgk1 served as loading control.

Figure S7

Table S1. Set of primers used in this study for qPCR or ChIP experiments.

Primers	Region/Locus	Sequence	Use
MC_636	ACT1 For	GGATTCTGGTATGTTCTAGCGCTTGCACCA	RT-qPCR and genomic DNA normalization
MC_637	ACT1 Rev	AATCTCTCGAGCAATTGGGACCGTGCA	RT-qPCR and genomic DNA normalization
MC_545	I-PpoI cut site For	TGTTGACGCAATGTGATTTCTGCCC	Genomic qPCR (DSB efficiency)
MC_546	I-PpoI cut site Rev	GTAGATAGGGACAGTGGGAATCTCG	Genomic qPCR (DSB efficiency)
MC_699	RDN1 #9 For	CTAGCGAAACCACAGCCAAG	ChIP normalization and control
MC_700	RDN1 #9 Rev	AATGTCTTCAACCCGGATCA	ChIP normalization and control
MC_701	RDN1 #12 For	TAATTGGTTTTTGCGGCTGT	ChIP normalization and RT-qPCR (control)
MC_702	RDN1 #12 Rev	ATGATTTATCCCCACGCAAA	ChIP normalization and RT-qPCR (control)
MC_387	RDN1 #15.1 For	TCACAAAGCTTCCCGAGCGTG	ChIP (binding site) and RT-qPCR (NTS1)
MC_388	RDN1 #15.1 Rev	TCATATCAAAGGCATGTCCTG	ChIP (binding site) and RT-qPCR (NTS1)
MC_393	RDN1 #23 For	GGGAGGTACTTCATGCGAAA	RT-qPCR (NTS2)
MC_394	RDN1 #23 Rev	AAGATGCCCACGATGAGACT	RT-qPCR (NTS2)
MC_711	RDN1 #25 For	GGCAGCAGAGAGACCTGAAA	ChIP normalization and genomic qPCR (rDNA copy number)
MC_712	RDN1 #25 Rev	GAGCCATTCGCAGTTTCACT	ChIP normalization and genomic qPCR (rDNA copy number)

Table S2. Yeast strains used in this study

Genotype	Source	Identifier
trp1-1 ura3-52 his3Δ200 leu2-3,11 lys2-801	Finley et al., 1987	DF5
DF5, MATα HEH1-L^{EGFP}::HIS3MX6	Capella et al., 2020	MC0064
DF5, MATa HEH1-L^{EGFP}::HIS3MX6 nur1Δ::kanMX6	This study	MC0479
DF5, MATa HEH1-L^{EGFP}::HIS3MX6 CSM1^{TAP}::kanMX6	This study	MC0659
DF5, MATa HEH1-L^{EGFP}::HIS3MX6 nur1Δ::kanMX6 CSM1^{TAP}::kanMX6	This study	MC0184
DF5, MATa LRS4^{3HA}::KITRP1	This study	MC0628
DF5, MATa LRS4^{3HA}::KITRP1 nur1Δ::kanMX6	This study	MC0682
DF5, MATα LRS4^{3HA}::KITRP1 natNT2::pHEH1::^{GFP}HEH1	This study	MC0656
DF5, MATa LRS4^{3HA}::KITRP1 natNT2::pHEH1::^{GFP}HEH1 nur1Δ::kanMX6	This study	MC0690
DF5, MATα natNT2::pMET25::^{yeGFP}LRS4	This study	MC0073
DF5, MATa natNT2::pMET25::^{yeGFP}LRS4 csm1Δ::hphNT1	This study	MC0089
DF5, MATa natNT2::pMET25::^{yeGFP}LRS4 NUR1^{3HA}::KITRP1	This study	MC0644
DF5, MATα natNT2::pMET25::^{yeGFP}LRS4 csm1Δ::hphNT1 NUR1^{3HA}::KITRP1	This study	MC0090
DF5, MATa natNT2::pMET25::^{yeGFP}LRS4 nur1Δ54^{3HA} (1-430aa)::KITRP1	This study	MC0607
DF5, MATa natNT2::pMET25::^{yeGFP}LRS4 nur1ΔC^{3HA} (1-295aa)::KITRP1	This study	MC0319
DF5, MATa CSM1^{TAP}::kanMX6	This study	MC0629
DF5, MATa HEH1-L^{EGFP}::HIS3MX6 CSM1^{TAP}::kanMX6 lrs4Δ::hphNT1	This study	MC0761
DF5, MATa HEH1-L^{EGFP} NUR1^{3HA}::KITRP1	This study	MC0660
DF5, MATa HEH1-L^{EGFP} nur1Δ54^{3HA} (1-430aa)::KITRP1	This study	MC0606
DF5, MATa HEH1-L^{EGFP} nur1ΔC^{3HA} (1-295aa)::KITRP1	This study	MC0318
DF5, MATa NET1::AIDx4^{9Myc}::HIS3MX6 URA3::pADH1::OsTIR1^{9Myc} Nur1^{3HA}::KITRP1	This study	MC0731
DF5, MATa NET1::AIDx4^{9Myc}::HIS3MX6 URA3::pADH1::OsTIR1^{9Myc} Nur1^{3HA}::KITRP1 natNT2::pMET25::^{yeGFP}LRS4	This study	MC0996
DF5, MATa NUR1^{3HA}::KITRP1	This study	MC0630
DF5, MATa HEH1-L^{EGFP} NUR1^{3HA}::KITRP1 lrs4Δ::hphNT1	This study	MC0760
DF5, MATa NUR1^{3HA}::KITRP1 URA3::pADH1::^{6His}SMT3	This study	MC0723
DF5, MATa HEH1-L^{EGFP} NUR1^{3HA}::KITRP1 URA3::pADH1::^{6His}SMT3	This study	MC0724
DF5, MATa natNT2::pMET25::^{yeGFP}LRS4 NUR1^{3HA}::KITRP1 URA3::pADH1::^{6His}SMT3	This study	MC0650
DF5, MATa NUR1^{3HA}::KITRP1 natNT2::pADH1::^{yeGFP}SMT3	This study	MC0076
DF5, MATa NUR1^{3HA}::KITRP1 siz1Δ::HIS3MX6	This study	MC0473
DF5, MATa NUR1^{3HA}::KITRP1 natNT2::pADH1::^{yeGFP}SMT3 siz1Δ::HIS3MX6	This study	MC0474
DF5, MATa NUR1^{3HA}::KITRP1 siz2Δ::HIS3MX6	This study	MC0475
DF5, MATa NUR1^{3HA}::KITRP1 natNT2::pADH1::^{yeGFP}SMT3 siz2Δ::HIS3MX6	This study	MC0476
DF5, MATa NUR1^{3HA}::KITRP1 sir2Δ::HIS3MX6	This study	MC0245
DF5, MATa NUR1^{3HA}::KITRP1 natNT2::pADH1::^{yeGFP}SMT3 sir2Δ::HIS3MX6	This study	MC0246
DF5, MATa NUR1^{3HA}::KITRP1 sir4Δ::hphNT1	This study	MC0811

DF5, MATa NUR1^{3HA}::KITRP1 natNT2::pADH1::^{yeGFP}SMT3 sir4Δ::hphNT1	This study	MC0812
DF5, MATa nur1Δ::kanMX6	This study	MC0634
DF5, MATa nur1Δ::kanMX6 natNT2::pADH1::^{yeGFP}SMT3	This study	MC0077
DF5, MATα URA3::pADH1::^{6His}SMT3	Paasch et al., 2018	MC0435
DF5, MATα heh1Δ::natNT2	Capella et al., 2020	MC0026
DF5, MATα lrs4Δ::hphNT1	This study	MC0429
DF5, MATa CSM1^{TAP}::kanMX6 heh1Δ::natNT2	This study	MC0692
DF5, MATa CSM1^{TAP}::kanMX6 URA3::pADH1::^{6His}SMT3	This study	MC0733
DF5, MATa natNT2::pMET25::^{yeGFP}LRS4 NUR1^{3HA}::KITRP1 slx8Δ::hphNT1	This study	MC0377
DF5, MATa natNT2::pMET25::^{yeGFP}LRS4 NUR1^{3HA}::KITRP1 slx5Δ::HIS3MX6 slx8Δ::hphNT1	This study	MC0378
MATa ADE2 RAD52^{YFP} RDN25::224xtetO-URA3-I-SceI TetI^{mRFP1}-iYGL119W	Torres-Rosell et al., 2007	ML118-1D
ML118-1D, MATa NUR1^{6HA}::HIS3MX6	This study	MC0857
ML118-1D, MATa nur1Δ54^{6HA} (1-430aa)::HIS3MX6	This study	MC0859
ML118-1D, MATa nur1ΔC^{6HA} (1-295aa)::HIS3MX6	This study	MC0860
ML118-1D, MATa nur1Δ::kanMX6	This study	MC0678
ML118-1D, MATa SMT3::kanMX6::pADH1::^{6His}SMT3	This study	MC0370
ML118-1D, MATa ufd1ΔSIM (1-355aa)::kanMX6	This study	MC0079
trp-901-, leu2-3,112 ura3-53 his3-200 gal4 gal80 GAL1::HIS GAL2- ADE2 met2::GAL7-lacZ	James et al., 1996	PJ69-7a
MATα ura3-52 his3-200 trp1-901 leu2-3,112 ade2-101 gal4Δ met– gal80Δ URA3::GAL1$_{UAS}$-GAL1$_{TATA}$::LacZ MEL1	Clontech®	Y187
MATa ura3-52 his3-200 trp1-901 leu2-3,112 gal4Δ gal80Δ LYS2::GAL1$_{UAS}$–GAL1$_{TATA::}$HIS3 GAL2$_{UAS}$–GAL2$_{TATA}$::ADE2 URA3::MEL1$_{UAS}$–MEL1$_{TATA::}$AUR1-C MEL1	Clontech®	Y2H Gold
ade2-1 can1-100 his3-11,15 leu2-3,112 trp1-1 ura3-1 RAD5	McDonald et al., 1997	W303 (RAD5)
W303, MATα natNT2::pMET25::^{yeGFP}LRS4	This study	MC0727
W303, MATα NET1^{EGFP}::HIS3MX6	This study	MC0836
W303, MATα TOF2^{EGFP}::HIS3MX6	This study	MC0837
W303, MATa NUR1^{6HA}::HIS3MX6	This study	MC0566
W303, MATa NUR1^{6HA}::HIS3MX6 natNT2::pMET25::^{yeGFP}LRS4	This study	MC0848
W303, MATα NUR1^{6HA}::HIS3MX6 natNT2::pMET25::^{yeGFP}LRS4 cdc14-3	This study	MC0938
W303, MATa NUR1^{6HA}::HIS3MX6 natNT2::pMET25::^{yeGFP}LRS4 cdc14-3	This study	MC0939
W303, MATa NUR1^{6HA}::HIS3MX6 natNT2::pMET25::^{yeGFP}LRS4 ufd1-2::kanMX6	This study	MC0462
W303, MATa NUR1^{6HA}::HIS3MX6 natNT2::pMET25::^{yeGFP}LRS4 ufd1ΔSIM (1-355aa)::kanMX6	This study	MC0478
W303, MATa NUR1^{6HA}::HIS3MX6 uls1Δ::kanMX6	This study	MC0117
W303, MATa NUR1^{6HA}::HIS3MX6 natNT2::pMET25::^{yeGFP}LRS4 uls1Δ::kanMX6	This study	MC0119
W303, MATa HEH1^{EGFP}::HIS3MX6	This study	MC0947
W303, MATa HEH1^{EGFP}::HIS3MX6 LRS4^{TAP}::kanMX6	This study	MC0948
W303, MATa HEH1^{EGFP}::HIS3MX6 LRS4^{TAP}::kanMX6 ChrIII$_{92.5kb}$::natNT2::pGALL::^{3HA}SV40 NLS-I-PPOI	This study	MC0991
W303, MATa HEH1^{EGFP}::HIS3MX6 LRS4^{TAP}::kanMX6 ChrIII$_{92.5kb}$::natNT2::pGALL::^{3HA}SV40 NLS-I-PPOI	This study	MC0992

W303, MATa NUR1^{6HA}::HIS3MX6 URA3::pGAL1::CDC48::ADHt	This study	MC0163
W303, MATa natNT2::pMET25::^{yeGFP}LRS4 URA3::pGAL1::CDC48::ADHt	This study	MC0164
W303, MATa NUR1^{6HA}::HIS3MX6 natNT2::pMET25::^{yeGFP}LRS4 URA3::pGAL1::CDC48::ADHt	This study	MC0165
W303, MATa NUR1^{6HA}::HIS3MX6 natNT2::pMET25::^{yeGFP}LRS4 URA3::pGAL1::cdc48-6::ADHt	This study	MC0168
W303, MATa NUR1^{6HA}::HIS3MX6 natNT2::pMET25::^{yeGFP}LRS4 URA3::pGAL1::cdc48 E588Q::ADHt	This study	MC0167
W303, MATa cdc48-3::LEU2	This study	MC0911
W303, MATa RDN1::ADE2	This study	MC0717
W303, MATa RDN1::ADE2 nur1Δ::kanMX6	This study	MC0669
W303, MATa RDN1::ADE2 lrs4Δ::hphNT1	This study	MC0641
W303, MATα RDN1::ADE2 ULP2^{6HA}::HIS3MX6	This study	MC0982
W303, MATα RDN1::ADE2 ulp2ΔC^{6HA} (1-781aa)::HIS3MX6	This study	MC0983
W303, MATa RDN1::Ade2 NUR1^{6HA}-ULP1-CD::HIS3MX6	This study	MC1032
W303, MATa RDN1::Ade2 NUR1^{6HA}-ulp1-CDi F474A C580S::HIS3MX6	This study	MC1033
W303, MATa RDN1::Ade2 NUR1^{3HA}::KITRP1	This study	MC0622
W303, MATa RDN1::Ade2 nur1 K175-176R^{3HA}::KITRP1	This study	MC0623
W303, MATa RDN1::Ade2 NUR1^{3HA}::KITRP1 rad52Δ::HIS3MX6	This study	MC0743
W303, MATa RDN1::Ade2 nur1 K175-176R^{3HA}::KITRP1 rad52Δ::HIS3MX6	This study	MC0744
W303, MATa RDN1::Ade2 NUR1^{6HA}::HIS3MX6	This study	MC0878
W303, MATa RDN1::Ade2 nur1 K175-176R^{6HA}::HIS3MX6	This study	MC0879
W303, MATa RDN1::Ade2 NUR1^{6HA}::HIS3MX6 lrs4Δ::hphNT1	This study	MC0880
W303, MATa RDN1::Ade2 nur1 K175-176R^{6HA}::HIS3MX6 lrs4Δ::hphNT1	This study	MC0881
W303, MATa RDN1::ADE2 ufd1ΔSIM (1-355aa)::kanMX6	This study	MC0160
W303, MATa RDN1::ADE2 ufd1ΔSIM (1-355aa)::kanMX6 lrs4Δ::hphNT1	This study	MC0161
W303, MATa RDN1::ADE2 ufd1ΔSIM (1-355aa)::kanMX6 nur1Δ::natNT2	This study	MC0994

References:

Capella, M., Caballero, L.M., Pfander, B., Braun, S., and Jentsch, S. (2020). ESCRT recruitment by the inner nuclear membrane protein Heh1 is regulated by Hub1-mediated alternative splicing. J. Cell Sci. jcs.250688.

Finley, D., Özkaynak, E., and Varshavsky, A. (1987). The yeast polyubiquitin gene is essential for resistance to high temperatures, starvation, and other stresses. Cell *48*, 1035–1046.

James, P., Halladay, J., and Craig, E.A. (1996). Genomic Libraries and a Host Strain Designed for Highly Efficient Two-Hybrid Selection in Yeast. Genetics *144*, 1425–1436.

McDonald, J.P., Levine, A.S., and Woodgate, R. (1997). The Saccharomyces cerevisiae RAD30 gene, a homologue of Escherichia coli dinB and umuC, is DNA damage inducible and functions in a novel error-free postreplication repair mechanism. Genetics *147*, 1557–1568.

Paasch, F., Den Brave, F., Psakhye, I., Pfander, B., and Jentsch, S. (2018). Failed mitochondrial

import and impaired proteostasis trigger SUMOylation of mitochondrial proteins. J. Biol. Chem. *293*, 599–609.

Torres-Rosell, J., Sunjevaric, I., De Piccoli, G., Sacher, M., Eckert-Boulet, N., Reid, R., Jentsch, S., Rothstein, R., Aragón, L., and Lisby, M. (2007). The Smc5-Smc6 complex and SUMO modification of Rad52 regulates recombinational repair at the ribosomal gene locus. Nat. Cell Biol. *9*, 923–931.

Table S3. Plasmids used in this study.

Point mutations refer to the position of the aminoacid/s (aa) in WT proteins. The specific positions of the truncated constructs are indicated in brackets.

Construct	Source	Identifier
YCplac22	Gietz and Akio, 1988	pMC_0111
YCplac22 pGAL1::HEH1-L-3HA-GBP::ADH1t	This study	pMC_0442
YCplac22 pNOP1::NOP1-ECFP	This study	pMC_0480
YCplac22 pGAL1::NUR1::ADH1t	This study	pMC_0595
YCplac22 pGAL1::nur1 S441D T446D S449D::ADH1t	This study	pMC_0599
YCplac22 pGAL1::nur1 S441A T446A S449A::ADH1t	This study	pMC_0600
YCplac111	Gietz and Akio, 1988	pMC_0110
YCplac111 pGAL1::yeGFP-HEH1-L::ADH1t	Capella et al., 2020	pMC_0395
YCplac111 pGAL1::yeGFP-LRS4::ADH1t	This study	pMC_0631
YCplac111 pGAL1::yeGFP-HEH1-L-LRS4::ADH1t	This study	pMC_0443
YCplac111 pGAL1::yeGFP-HEH1-L-lrs4 Δ1-35aa::ADH1t	This study	pMC_0444
YCplac111 pGAL1::yeGFP-HEH1-L-lrs4 Q325Stop::ADH1t	This study	pMC_0445
YCplac111 pGAL1::yeGFP-HEH1-L-TOF2::ADH1t	This study	pMC_0446
YCplac111 pGAL1::yeGFP-HEH1-L-GAL4-BD::ADH1t	This study	pMC_0447
YCplac111 pGALS::yeGFP-HEH1-L-LRS4::ADH1t	This study	pMC_0448
YCplac111 pNUR1::NUR1::ADH1t	This study	pMC_0565
YCplac111 pNUR1::nur1 S441D T446D S449D::ADH1t	This study	pMC_0570
YCplac111 pNUR1::NUR1-TAP::ADH1t	This study	pMC_0565
YCplac111 pNUR1::nur1 S441D T446D S449D-TAP::ADH1t	This study	pMC_0570
YCplac111 pNUR1::NUR1-3HA	This study	pMC_0545
YCplac111 pNUR1::nur1 K175-176R-3HA	This study	pMC_0546
YCplac111 pNUR1::nur1 K306R-3HA	This study	pMC_0547
YCplac111 pNUR1::nur1 K353R-3HA	This study	pMC_0548
YCplac111 pNUR1::nur1 K465R-3HA	This study	pMC_0549
YCplac111 pNUR1::nur1 K477R-3HA	This study	pMC_0550
YCplac111 pNUR1::smt3 Q95P-NUR1-3HA	This study	pMC_0555
YCplac111 pNUR1::smt3 F37A I39A Q95P-NUR1-3HA	This study	pMC_0556
YCplac111 pLRS4::LRS4-TAP::ADH1t	This study	pMC_0637
YCplac111 pLRS4::smt3 Q95P-LRS4-TAP::ADH1t	This study	pMC_0638
YCplac111 pLRS4::smt3 F37A I39A Q95P-LRS4-TAP::ADH1t	This study	pMC_0639
YCplac111 pNUR1::NUR1-3HA	This study	pMC_0545
YCplac111 pNUR1::smt3 Q95P-NUR1-3HA	This study	pMC_0555
YCplac111 pNUR1::smt3 F37A I39A Q95P-NUR1-3HA	This study	pMC_0546
YCplac111 pGAL1::2xSV40 NLS-HA-I-SceI::ADH1t	This study	pMC_0298
pRS415 pGAL1	Mumberg et al., 1995	pMC_0147
pRS415 pGAL1::3HA-I-PpoI-GR-LBD::CYC1t	This study	pMC_0320
pRS415 pTEF1	This study	pMC_0485
pRS415 pTEF1::SMT3 GG::CYC1t	This study	pMC_0486
pCu415 pGAL1::SMT3 GG::CYC1t	Fabian den Brave, University of Bonn	pMC_0197
pCu415 pGAL1::smt3 Q95P GG::CYC1t	Fabian den Brave, University of Bonn	pMC_0200

pCu415 pGAL1::smt3 F37A I39A GG::CYC1t	Fabian den Brave, University of Bonn	pMC_0199
pCu415 pGAL1::smt3 KRall GG::CYC1t	Fabian den Brave, University of Bonn	pMC_0201
pGBKT7	Clontech®	pMC_0385
pGBKT7 CSM1	This study	pMC_0477
pGBKT7 LRS4	This study	pMC_0479
pGBKT7 CDC14	This study	pMC_0658
pGBKT7 SMT3 AA	This study	pMC_0273
pGBKT7 smt3 F37A I39A AA	This study	pMC_0275
pGADT7	Clontech®	pMC_0386
pGADT7 HEH1 N (1-454aa)	Capella et al., 2020	pMC_0354
pGADT7 HEH1 C (730-834aa)	Capella et al., 2020	pMC_0355
pGADT7 NUR1 N (1-60aa)	This study	pMC_0505
pGADT7 NUR1 M (167-240aa)	This study	pMC_0507
pGADT7 NUR1 C (278-484aa)	This study	pMC_0504
pGADT7 NUR1 278-332 (278-332aa)	This study	pMC_0524
pGADT7 NUR1 278-430 (278-430aa)	This study	pMC_0523
pGADT7 NUR1 333-484 (333-484aa)	This study	pMC_0525
pGADT7 NUR1 431-484 (431-484aa)	This study	pMC_0527
pGADT7 NUR1 333-430 (333-430aa)	This study	pMC_0526
pGADT7 NUR1 S441D T446D (278-484aa)	This study	pMC_0529
pGADT7 NUR1 S439D S441D T446D (278-484aa)	This study	pMC_0535
pGADT7 NUR1 S441D T446D S449D (278-484aa)	This study	pMC_0537
pGADT7 NUR1 S439D S441D T446D S449D (278-484aa)	This study	pMC_0539
pGADT7 NUR1 S441A T446A (278-484aa)	This study	pMC_0530
pGADT7 NUR1 S439A S441A T446A (278-484aa)	This study	pMC_0536
pGADT7 NUR1 S441A T446A S449A (278-484aa)	This study	pMC_0538
pGADT7 NUR1 S439A S441A T446A S449A (278-484aa)	This study	pMC_0540
pGADT7 SMT3 GG	This study	pMC_0276
pGADT7 SMT3 AA	This study	pMC_0277
pGADT7 CDC48	This study	pMC_0470
pGADT7 NPL4	This study	pMC_0472
pGADT7 UFD1	This study	pMC_0473
pGADT7 ufd1ΔSIM (1-355aa)	This study	pMC_0474

References

Capella, M., Caballero, L.M., Pfander, B., Braun, S., and Jentsch, S. (2020). ESCRT recruitment by the inner nuclear membrane protein Heh1 is regulated by Hub1-mediated alternative splicing. J. Cell Sci. jcs.250688.

Gietz, R.D., and Akio, S. (1988). New yeast-Escherichia coli shuttle vectors constructed with in vitro mutagenized yeast genes lacking six-base pair restriction sites. Gene *74*, 527–534.

Mumberg, D., Müller, R., and Funk, M. (1995). Yeast vectors for the controlled expression of heterologous proteins in different genetic backgrounds. Gene *156*, 119–122.

Table S4

Rates of *ADE2* marker loss from rDNA repeats.

Figure	Genotype	Name	Repl	Half-red colonies	Total colonies (w/o fully red)	Rate of loss	rel. to WT	log2 (Ratio)	rel. to mean of WT
3C	*RDN1::ADE2 + YCplac111*	**WT**	1	63	5793	0.01	**1.00**	-6.52	0.12
			2	48	5039	0.01		-6.71	-0.07
			3	41	4897	0.01		-6.90	-0.25
			4	56	4908	0.01		-6.45	0.19
	RDN1::ADE2 nur1Δ::kanMX6 + YCplac111	***nur1Δ* + Empty**	1	112	5419	0.02	**1.88**	-5.60	1.05
			2	88	5107	0.02		-5.86	0.79
			3	80	4534	0.02		-5.82	0.82
			4	100	5017	0.02		-5.65	1.00
	RDN1::ADE2 nur1Δ::kanMX6 + YCplac111 pNUR1::NUR1::ADH1t	***nur1Δ + NUR1***	1	55	6839	0.01	**0.84**	-6.96	-0.31
			2	57	7343	0.01		-7.01	-0.36
			3	56	5817	0.01		-6.70	-0.05
	RDN1::ADE2 nur1Δ::kanMX6 + YCplac111 pNUR1::nur1 S441D T446D S449D::ADH1t	***nur1Δ + nur1Pmim***	1	94	6156	0.02	**1.58**	-6.03	0.61
			2	96	5872	0.02		-5.93	0.71
			3	96	5983	0.02		-5.96	0.69

Figure	Genotype	Name	Repl	Half-red colonies	Total colonies (w/o fully red)	Rate of loss	rel. to WT	log2 (Ratio)	rel. to mean of WT
4B	*RDN1::ADE2 + pRS415 pGAL1*	**WT**	1	10	4825	0.00	**1.00**	-8.91	-0.38
			2	26	8143	0.00		-8.29	0.24
			3	18	6689	0.00		-8.54	-0.01
			4	14	4656	0.00		-8.38	0.15
	RDN1::ADE2 + pCu415 pGAL1::SMT3 GG::CYC1t	**SUMO-OE**	1	15	3827	0.00	**2.22**	-8.00	0.54
			2	35	6171	0.01		-7.46	1.07
			3	38	7081	0.01		-7.54	0.99
			4	42	4464	0.01		-6.73	1.80
	RDN1::ADE2 lrs4Δ::hphNT1 + pRS415 pGAL1	***lrs4Δ***	1	75	5594	0.01	**5.72**	-6.22	2.31
			2	48	2673	0.02		-5.80	2.73
	RDN1::ADE2 lrs4Δ::hphNT1 + pRS415 pGAL1::SMT3 GG::CYC1t	**SUMO-OE *lrs4Δ***	1	83	5513	0.02	**6.43**	-6.05	2.48
			2	73	3620	0.02		-5.63	2.90

Figure	Genotype	Name	Repl	Half-red colonies	Total colonies (w/o fully red)	Rate of loss	rel. to WT	log2 (Ratio)	rel. to mean of WT
S4B	*RDN1::ADE2 ULP2^{6HA}::HIS3MX6*	**WT**	1	31	10101	0.00	**1.00**	-8.35	0.07
			2	19	6255	0.00		-8.36	0.05
			3	24	8865	0.00		-8.53	-0.12
	RDN1::ADE2 ULP2ΔC^{6HA} (1-781aa)::HIS3MX6	***ulp2ΔC***	1	50	9591	0.01	**2.16**	-7.58	0.83
			2	67	9367	0.01		-7.13	1.29
			3	55	8287	0.01		-7.24	1.18

Figure	Genotype	Name	Repl	Half-red colonies	Total colonies (w/o fully red)	Rate of loss	rel. to WT	log2 (Ratio)	rel. to mean of WT
5D left	*RDN1::ADE2 NUR^{6HA}::HIS3MX6*	**WT**	1	101	7211	0.01	**1.00**	-6.16	0.40
			2	41	6458	0.01		-7.30	-0.74
			3	93	7762	0.01		-6.38	0.17
			4	68	5659	0.01		-6.38	0.18
	RDN1::ADE2 NUR K175-176R^{6HA}::HIS3MX6	***nur1KR***	1	46	10001	0.00	**0.33**	-7.76	-1.21
			2	20	8787	0.00		-8.78	-2.22
			3	38	8771	0.00		-7.85	-1.30
			4	23	6405	0.00		-8.12	-1.57
	RDN1::ADE2 NUR^{6HA}::HIS3MX6 lrs4Δ::hphNT1	***lrs4Δ***	1	129	6534	0.02	**2.05**	-5.66	0.89
			2	159	6153	0.03		-5.27	1.28
			3	123	5239	0.02		-5.41	1.14
			4	132	5991	0.02		-5.50	1.05
	RDN1::ADE2 NUR K175-176R^{6HA}::HIS3MX6 lrs4Δ::hphNT1	***nur1KR lrs4Δ***	1	129	5588	0.02	**2.03**	-5.44	1.12
			2	145	7978	0.02		-5.78	0.77
			3	96	5371	0.02		-5.81	0.75
			4	147	4783	0.03		-5.02	1.53

Figure	Genotype	Name	Repl	Half-red colonies	Total colonies (w/o fully red)	Rate of loss	rel. to WT	log2 (Ratio)	rel. to mean of WT
5D right	*RDN1::ADE2 NUR^{3HA}::KlTRP1*	**WT**	1	13	5039	0.00	**1.00**	-8.60	0.07
			2	10	4953	0.00		-8.95	-0.29
			3	5	1748	0.00		-8.45	0.22
	RDN1::ADE2 NUR K175-176R^{3HA}::KlTRP1	***nur1KR***	1	8	5029	0.00	**0.55**	-9.30	-0.63
			2	5	5114	0.00		-10.00	-1.33
			3	3	1930	0.00		-9.33	-0.66
	RDN1::ADE2 NUR^{3HA}::KlTRP1 rad52Δ::HIS3MX6	***rad52Δ***	1	4	2883	0.00	**0.61**	-9.49	-0.83
			2	4	2826	0.00		-9.46	-0.80
			3	2	1142	0.00		-9.16	-0.49
	RDN1::ADE2 NUR K175-176R^{3HA}::KlTRP1 rad52Δ::HIS3MX6	***nur1KR rad52Δ***	1	5	2913	0.00	**0.53**	-9.19	-0.52
			2	3	2354	0.00		-9.62	-0.95
			3	1	1048	0.00		-10.03	-1.37

Figure	Genotype	Name	Repl	Half-red colonies	Total colonies (w/o fully red)	Rate of loss	rel. to WT	log2 (Ratio)	rel. to mean of WT
5E left	*RDN1::ADE2 nur1Δ::kanMX6 + YCplac111 pNUR1::NUR1-3HA::ADH1t*	***nur1Δ + NUR1***	1	44	6287	0.01	**1.00**	-7.16	0.20
			2	36	6353	0.01		-7.46	-0.11
			3	40	6014	0.01		-7.23	0.12
			4	36	6857	0.01		-7.57	-0.22
	RDN1::ADE2 nur1Δ::kanMX6 + YCplac111 pNUR1::smt3 Q95P-NUR1-3HA::ADH1t	***nur1Δ + SUMO-NUR1***	1	68	7204	0.01	**1.98**	-6.73	0.63
			2	87	7896	0.01		-6.50	0.85
			3	78	6236	0.01		-6.32	1.04
			4	95	6083	0.02		-6.00	1.36
	RDN1::ADE2 nur1Δ::kanMX6 + YCplac111 pNUR1::smt3 F37A I39A Q95P-NUR1-3HA::ADH1t	***nur1Δ + SUMO^{FAIA}-NUR1***	1	40	5968	0.01	**1.19**	-7.22	0.14
			2	39	6598	0.01		-7.40	-0.05
			3	47	5707	0.01		-6.92	0.43
			4	52	6255	0.01		-6.91	0.45

Figure	Genotype	Name	Repl	Half-red colonies	Total colonies (w/o fully red)	Rate of loss	rel. to WT	log2 (Ratio)	rel. to mean of WT
			1	56	5855	0.01		-6.71	0.33

5E right	*RDN1::ADE2 lrs4Δ::hphNT1 + YCplac111 pLRS4::LRS4-TAP::ADH1t*	***lrs4Δ + LRS4***	2	42	6852	0.01	**1.00**	-7.35	-0.31
			3	44	5880	0.01		-7.06	-0.02
	RDN1::ADE2 lrs4Δ::hphNT1 + YCplac111 pLRS4::smt3 Q95P-LRS4-TAP::ADH1t	***lrs4Δ + SUMO-LRS4***	1	94	4823	0.02	**1.94**	-5.68	1.36
			2	82	5339	0.02		-6.02	1.02
			3	79	6384	0.01		-6.34	0.70
			4	88	6843	0.01		-6.28	0.76
	RDN1::ADE2 lrs4Δ::hphNT1 + YCplac111 pLRS4::smt3 F37A I39A Q95P-LRS4-TAP::ADH1t	***lrs4Δ + SUMO^{FAIA}-LRS4***	1	49	5573	0.01	**0.91**	-6.83	0.21
			2	40	5219	0.01		-7.03	0.01
			3	38	5799	0.01		-7.25	-0.21
			4	34	6815	0.00		-7.65	-0.61
	RDN1::ADE2 lrs4Δ::hphNT1 + YCplac111	***lrs4Δ* + Empty**	1	68	2931	0.02	**2.73**	-5.43	1.61
			2	114	6097	0.02		-5.74	1.30
			3	110	5163	0.02		-5.55	1.49

Figure	Genotype	Name	Repl	Half-red colonies	Total colonies (w/o fully red)	Rate of loss	rel. to WT	log2 (Ratio)	rel. to mean of WT
S5H left	*RDN1::ADE2 NUR^{6HA}::HIS3MX6 + pRS415 pGAL1*	**WT**	1	57	6540	0.01	**1.00**	-6.84	-0.12
			2	57	6875	0.01		-6.91	-0.20
			3	74	5960	0.01		-6.33	0.39
			4	67	7385	0.01		-6.78	-0.07
	RDN1::ADE2 NUR^{6HA}::HIS3MX6 + pCu415 pGAL1::SMT3 GG::CYC1t	**SUMO-OE**	1	106	5760	0.02	**2.32**	-5.76	0.95
			2	122	6705	0.02		-5.78	0.94
			3	112	3810	0.03		-5.09	1.63
			4	147	6299	0.02		-5.42	1.30
	RDN1::ADE2 NUR K175-176R^{6HA}::HIS3MX6 + pRS415 pGAL1	***nur1KR***	1	34	7209	0.00	**0.50**	-7.73	-1.01
			2	32	7826	0.00		-7.93	-1.22
			3	36	6434	0.01		-7.48	-0.76
			4	35	7434	0.00		-7.73	-1.01
	RDN1::ADE2 NUR K175-176R^{6HA}::HIS3MX6 + pCu415 pGAL1::SMT3 GG::CYC1t	**SUMO-OE *nur1KR***	1	60	6366	0.01	**1.21**	-6.73	-0.01
			2	57	6179	0.01		-6.76	-0.04
			3	82	5265	0.02		-6.00	0.71
			4	55	4485	0.01		-6.35	0.37

Figure	Genotype	Name	Repl	Half-red colonies	Total colonies (w/o fully red)	Rate of loss	rel. to WT	log2 (Ratio)	rel. to mean of WT
S5H right	*RDN1::ADE2 NUR1^{6HA}-ulp1-CDi F474A C580S::HIS3MX6*	**Nur1-uD^{i}**	1	119	8686	0.01	**1.00**	-6.19	-0.01
			2	123	8269	0.01		-6.07	0.10
			3	114	8647	0.01		-6.25	-0.07
			4	110	8076	0.01		-6.20	-0.02
	RDN1::ADE2 NUR1^{6HA}-ULP1-CD::HIS3MX6	**Nur1-UD**	1	101	9587	0.01	**0.77**	-6.57	-0.39
			2	95	8180	0.01		-6.43	-0.25
			3	81	7846	0.01		-6.60	-0.42
			4	73	7330	0.01		-6.65	-0.47

Figure	Genotype	Name	Repl	Half-red colonies	Total colonies (w/o fully red)	Rate of loss	rel. to WT	log2 (Ratio)	rel. to mean of WT
6G left	*RDN1::ADE2*	**WT**	1	29	10149	0.00	**1.00**	-8.45	-0.36
			2	42	11890	0.00		-8.15	-0.05
			3	56	11442	0.00		-7.67	0.42
	RDN1::ADE2 UFD1ΔSIM (1-355aa)::kanMX6	***ufd1ΔSIM***	1	14	11305	0.00	**0.41**	-9.66	-1.57
			2	13	12724	0.00		-9.93	-1.84
			3	27	11213	0.00		-8.70	-0.61
	RDN1::ADE2 lrs4Δ::hphNT1	***lrs4Δ***	1	101	5515	0.02	**4.90**	-5.77	2.32
			2	90	5476	0.02		-5.93	2.16
			3	100	4863	0.02		-5.60	2.49
	RDN1::ADE2 UFD1ΔSIM (1-355aa)::kanMX6 lrs4Δ::hphNT1	***lrs4Δ ufd1ΔSIM***	1	96	5723	0.02	**4.93**	-5.90	2.19
			2	104	5282	0.02		-5.67	2.42
			3	96	4996	0.02		-5.70	2.39

Figure	Genotype	Name	Repl	Half-red colonies	Total colonies (w/o fully red)	Rate of loss	rel. to WT	log2 (Ratio)	rel. to mean of WT
6G right	*RDN1::ADE2 + pRS415 pTEF1*	**WT**	1	33	6339	0.01	**1.00**	-7.59	-0.44
			2	64	6917	0.01		-6.76	0.39
			3	43	5825	0.01		-7.08	0.06
	RDN1::ADE2 + pRS415 pTEF1::SMT3 GG::CYC1t	**SUMO-OE**	1	105	7158	0.01	**2.15**	-6.09	1.05
			2	130	6469	0.02		-5.64	1.50
			3	67	5538	0.01		-6.37	0.77
	RDN1::ADE2 ufd1ΔSIM (1-355aa)::kanMX6 + pRS415 pTEF1	***ufd1ΔSIM***	1	11	6614	0.00	**0.33**	-9.23	-2.09
			2	9	2613	0.00		-8.18	-1.04
			3	16	6169	0.00		-8.59	-1.45
			4	11	5507	0.00		-8.97	-1.83
	RDN1::ADE2 ufd1ΔSIM (1-355aa)::kanMX6 + pRS415 pTEF1::SMT3 GG::CYC1t	***ufd1ΔSIM* SUMO-OE**	1	26	6728	0.00	**0.45**	-8.02	-0.87
			2	14	3645	0.00		-8.02	-0.88
			3	19	6382	0.00		-8.39	-1.25
			4	13	5594	0.00		-8.75	-1.61

Figure	Genotype	Name	Repl	Half-red colonies	Total colonies (w/o fully red)	Rate of loss	rel. to WT	log2 (Ratio)	rel. to mean of WT
6H	*RDN1::ADE2 nur1Δ::kanMX6 + YCplac22 pGAL1::NUR1::ADHt*	***nur1Δ + NUR1***	1	192	5010	0.04	**1.00**	-4.71	0.03
			2	131	3880	0.03		-4.89	-0.15
			3	166	4085	0.04		-4.62	0.12
	RDN1::ADE2 nur1Δ::kanMX6 + YCplac22 pGAL1::nur1 S441A T446A S449A::ADHt	***nur1Δ + nur1Pmut***	1	116	4921	0.02	**0.47**	-5.41	-0.67
			2	52	3900	0.01		-6.23	-1.49
			3	65	3937	0.02		-5.92	-1.18
	RDN1::ADE2 nur1Δ::natNT2 ufd1ΔSIM::kanMX6 + YCplac22 pGAL1::NUR1::ADHt	***nur1Δ ufd1ΔSIM + NUR1***	1	29	5242	0.01	**0.17**	-7.50	-2.76
			2	31	4134	0.01		-7.06	-2.32
			3	26	3952	0.01		-7.25	-2.51
	RDN1::ADE2 nur1Δ::natNT2 ufd1ΔSIM::kanMX6 + YCplac22 pGAL1::nur1 S441A T446A S449A::ADHt	***nur1Δ ufd1ΔSIM + nur1Pmut***	1	49	4919	0.01	**0.22**	-6.65	-1.91
			2	36	4398	0.01		-6.93	-2.19
			3	26	3952	0.01		-7.25	-2.51